Experiments on Entrainment of Tailings into Suspension in an Annular Flume

Andrés F. Rojas-Aguirre, Ph.D.[1]; and Marcelo H. Garcia, Ph.D., Dist.M.ASCE[2]

Abstract: Sediment entrainment formulations developed for noncohesive materials have been widely applied to determine suspended loads in fluvial environments. Most relations were developed based on laboratory experiments and field measurements taken in sand-rich environments. Due to the accidental discharge of mine tailings in riverine systems, it is imperative to develop new approaches to predict sediment entrainment and resulting near-bed concentrations, as field observations show that the primary mode of transport for tailings once they are eroded is in suspension. Based on laboratory experiments conducted with poorly sorted iron tailings samples in an annular flume, we found that existing sand-based relations predict relatively well equilibrium near-bed concentrations when treated as well-sorted material. However, to predict entrainment rates into suspension for the tested poorly sorted iron tailings samples, sand-based entrainment relations require adding two functions accounting for the relative roughness of the bed material and the Reynolds particle number for the effect of viscous sublayer thickness on entraining fine grains. This innovative approach, combining dimensional analysis, similarity parameters, and experimental observations in an annular flume, provides a general framework for developing formulations to estimate the flow conditions necessary to entrain into suspension and then transport tailings either accidentally released into riverine environments or resuspended during dredging operations in watercourses. **DOI: 10.1061/JHEND8.HYENG-14095.**

Introduction

Research on tailings erosion has mainly focused on determining the resuspension of impoundment tailings caused by wind-induced waves in mine ponds (Adu-Wusu et al. 2001; Mian and Yanful 2004; Yanful and Catalan 2002; Geremew 2017). These quiescent mine ponds are used to properly dispose of and reduce tailings oxidation to avoid contamination of the surroundings. Accidents at mining facilities or improper disposal of tailings has dumped a considerable volume of these materials along river networks, impairing their water uses in the downstream direction (Macklin et al. 2003; Simeoni et al. 2017; do Carmo et al. 2017; Hudson-Edwards et al. 2003; Thompson et al. 2020). Extensive databases of these accidents have been developed by different agencies, such as the WISE Uranium Project (WISE 2022), the International Committee of Large Dams (ICOLD 2001), the United Nations (UNEP 1996), and other research studies (Azam and Li 2010; Armstrong et al. 2019; Piciullo et al. 2022).

Despite the multiple accidents reported in these databases, it was not until the collapse of Fundão dam (2015 in Mariana, Brazil) and Dam B1 at the Córrego de Feijão mine (2019 in Brumadinho, Brazil) that risk assessment began to have notable importance worldwide with the goal of minimizing future catastrophic events that could lead to life losses and environmental impacts along watercourses (Piciullo et al. 2022). Following these accidents, several studies have focused on reproducing and assessing the risk of large-scale tailings flows immediately after a tailings dam breach (Lumbroso et al. 2021; Ghahramani et al. 2022; Martínez-Aranda et al. 2022; Ghahramani et al. 2022). However, the spreading of tailings that reach a watercourse is usually quantitatively assessed using hydrodynamic and classical sediment transport models (Ferguson and Church 2004; Cao and Pender 2004; Pickup and Cui 2008).

To adequately predict the suspended tailings loads in watercourses, a sediment erosion equation must be implemented to determine the tailings entrainment rates from the bed into the water column. However, no research has been conducted to analyze the erosion of tailings mixtures subjected to fluvial conditions. As a result, no formulations have been developed to predict near-bed tailings concentrations. This provided the motivation for the work presented herein. The main objective was to assess the suitability of sand-based formulations for predicting the near-bed concentrations in an iron tailings riverbed, based on two iron tailings samples subjected to multiple bed shear stresses in an annular flume. The potential relevance of flocculation and hindered processes was also evaluated by conducting experiments in a settling column for different initial tailings concentrations. Finally, new entrainment formulations for poorly sorted iron ore tailings, which include the effects of a viscous sublayer thickness and relative roughness, were developed with the help of dimensional analysis, similarity parameters, and experimental observations made in an annular flume.

Theoretical Considerations

Mine tailings are commonly classified and treated as cohesive sediment due to the high amount of fine material (clay and silt-sized), in which the interparticle forces dominate the erosion behavior (Geremew and Yanful 2011). Haneef-Mian et al. (2007) found that

[1]Postdoctoral Research Associate, Dept. of Civil and Environmental Engineering, Ven Te Chow Hydrosystems Laboratory, Univ. of Illinois at Urbana-Champaign, Urbana, IL 61801; formerly, Postdoctoral Research Fellow, School of the Environment, San Francisco State Univ., San Francisco, CA 94132 (corresponding author). ORCID: https://orcid.org/0009-0006-9085-2881. Email: afr3@illinois.edu

[2]Professor, Director, and M. T. Geoffrey Yeh Endowed Chair, Dept. of Civil and Environmental Engineering, Ven Te Chow Hydrosystems Laboratory, Univ. of Illinois at Urbana-Champaign, Urbana, IL 61801. ORCID: https://orcid.org/0000-0003-0643-489X

Note. This manuscript was submitted on February 8, 2024; approved on September 9, 2024; published online on November 15, 2024. Discussion period open until April 15, 2025; separate discussions must be submitted for individual papers. This paper is part of the *Journal of Hydraulic Engineering*, © ASCE, ISSN 0733-9429.

the rate of erosion in lead-zinc mine tailings can be predicted by using the fine-grained cohesive sediment formulations derived for cohesive natural sediments (Ariathurai and Krone 1976; Hayter and Mehta 1986; Mehta and McAnally 2008), such as

$$E = \alpha\left(\frac{\tau - \tau_{cr}}{\tau_{cr}}\right)^{\theta} \quad (1)$$

where E = erosion rate $[ML^{-2}T^{-1}]$; τ_{cr} = critical shear stress $[ML^{-1}T^{-2}]$; τ = exerted shear stress; and θ and α are coefficients determined by regression from erosion measurements.

Using tailings with different physical, chemical, and mineralogical compositions, Geremew and Yanful (2011) found a transition from cohesive to noncohesive behavior when the content of fines (<63 μm) is in a range between $\phi_{fines} = 50\%$ to $\phi_{fines} = 55\%$, and therefore, Eq. (1) is valid when fine fractions are above this threshold. Conversely, when $\phi_{fines} < 50\%$, noncohesive erosion equations would be expected to be adequate to predict the erosion of such materials.

The erosion rate E can be used in a sediment transport model to estimate the erosion flux $E_r = E/\rho$ $[LT^{-1}]$. Thus, for a turbulent flow over an erodible tailings bed, the net upward volume flux of suspended sediment, F, is estimated as (Garcia and Parker 1991)

$$F = E_r - D_r \quad (2)$$

where E_r and D_r = erosion and settling fluxes $[LT^{-1}]$, respectively.

For the case of granular mixtures, the net upward sediment flux of suspended sediment in the ith grain size range at a small vertical distance close to the bed (reference height-a) takes the form

$$F_{ai} = v_{si}(F_i E_{si} - f_{ai} C_a) \quad (3)$$

where F_{ai} = net upward volume flux of suspended sediment at a for grain size i; E_{si} = dimensionless entrainment of the bed sediment into suspension at a for grain size i; f_{ai} = volume fraction of the suspended material at a for grain size i; F_i = volume fraction of the bed material for grain size i; v_{si} = settling velocity for grain size i; and C_a = total concentration of suspended sediment at $z = a$.

For cohesionless sediment, during equilibrium conditions, the upward flux due to the effect of turbulence is balanced with the settling due to gravity, leading to an equilibrium suspended sediment concentration condition. Therefore, E_{si} is determined as a function of the concentration and fractions at the reference height (a) and the fractions in the bed (F_i) as the upward volume fluxes F_{ai} are assumed to be negligible in Eq. (3) (i.e., $F_{ai} = 0$)

$$E_{si} = \frac{f_{ai} C_a}{F_i} = \frac{C_{ai}}{F_i} \quad (4)$$

Assuming equilibrium conditions, Rouse's theory for suspensions can be implemented to determine the suspended sediment in the vertical direction for steady and uniform flow (Vanoni 2006)

$$\frac{C_{zi}}{C_{ai}} = \left(\frac{H - z}{z}\frac{a}{H - a}\right)^{Z_{Ri}} \quad (5)$$

where C_{zi} = volumetric sediment concentration at a dimensionless vertical distance from the bed (z) for grain size i; a = reference height; and Z_{Ri} = Rouse Number for grain size i defined as

$$Z_{Ri} = \frac{v_{si}}{\beta \kappa u_*} \quad (6)$$

where κ = von Karman's constant equal to 0.41; u_* = shear velocity; and β is a dimensionless ratio that relates the turbulent diffusivity of the sediment (ϵ_s) to the turbulent eddy viscosity (ν_t). Thus, this term can also be expressed as the inverse of the Schmidt number, $\sigma_t = 1/\beta$ (Lyn 2008).

According to Graf and Cellino (2010) the β values can be $\beta > 1$ in the presence of bedforms, or $\beta < 1$, otherwise. Wright and Parker (2003) found that $\beta < 1$ is relevant in low-slope, large rivers due to the sediment induced stratification effects. De Leeuw et al. (2020) found that $\beta = 0.94$ is an adequate value based on field and experimental measurements. Some formulations available in the literature to estimate β are reported in Table 1. They include those of van Rijn (1984), Wright and Parker (2005), and De Leeuw et al. (2020).

The formulations in the literature to estimate the near-bed sediment concentration (or the entrainment in equilibrium conditions) for noncohesive materials are primarily based on natural sediments in the sand and gravel size ranges (Table 2). These formulations assume that flocculation and hindered settling processes are negligible. They are based on dimensionless analysis that can be explained and expressed by combining different dimensionless parameters Π_i (Parker and Anderson 1977), as follows:

$$E_{si} = f(\Pi_1, \Pi_2, \Pi_3, \Pi_4) \quad (7a)$$

$$\Pi_1: \tau^*_{si} = \frac{\tau_{bs}}{R_i g D_i} \quad \text{or} \quad \frac{u_*}{v_{si}} \quad \text{or} \quad \frac{u^*_s}{v_{si}} \quad (7b)$$

$$\Pi_2: R_{epi} = \frac{\sqrt{R_i g D_i} D_i}{\nu} \quad \text{or} \quad D^* = R_{epi}^{2/3} \quad (7c)$$

$$\Pi_3: \frac{D_i}{D_g} \quad \text{or} \quad \frac{D_i}{D_{50}} \quad (7d)$$

$$\Pi_4: \text{Hydraulic Parameters}\left(e.g. \ Fr \quad \text{or} \quad C_f \quad \text{or} \quad S \quad \text{or} \quad \frac{H}{k_s}\right) \quad (7e)$$

where D_i = diameter for grain size i; D_g = geometric mean diameter; D_{50} = grain size for which 50% of the material is finer; D^* = dimensionless particle diameter; u_* = shear velocity; u^*_s = shear velocity due to the skin friction component; R_i = submerged specific gravity for grain size i; ν = kinematic viscosity; τ_{bs} = bed shear stress due to the skin friction component; τ^*_{si} = Shields stress number due to the skin friction component for grain size i; Re_{pi} = particle Reynolds number grain size i; Fr = Froude number; S = longitudinal energy slope; C_f = friction coefficient; H = water depth; k_s = Nikuradse's roughness; g = acceleration of gravity equal to 9.81 m/s^2; and v_{si} = settling velocity for grain size i. Although there are various formulations for estimating v_{si}, in this study we used the equation derived by Ferguson and Church (2004)

$$v_{si} = \frac{R_i g D_i^2}{C_1 \nu + (0.75 C_2 R_i g D_i^3)^{0.5}} \quad (8)$$

where $C_1 = 18$; and $C_2 = 1$.

Table 1. Formulations to estimate β factor

Authors	Equations
van Rijn (1984)	$\beta = 1 + 2(v_s/u_*)^2$ if $0.1 < \frac{v_s}{u_*} < 1.0$
Wright and Parker (2005)	$\beta = 1 - 0.06(C_a/S)^{0.77}$ if $(C_a/S) < 10$ $\beta = 0.67 - 0.0025(C_a/S)$ if $(C_a/S) > 10$
De Leeuw et al. (2020)	$\beta = 16.82(u^*_s/v_{si})^{-0.54} C_f^{0.3}$

Table 2. Sediment entrainment formulations

Authors	Equations	Reference height a	Grain size distributions
Smith and McLean (1977)	$E_s = \frac{0.65\gamma_0 S_0}{1+\gamma_0 S_0}$ $S_0 = \frac{\tau_s^* - \tau_c^*}{\tau_c^*}, \gamma_0 = 2.4\times 10^{-3}$	$a = \alpha_0(\tau_s^* - \tau_c^*)D_s + k_s$ $\alpha_0 = 26.3$	Uniform
van Rijn (1984)	$E_s = 0.015\frac{D_s}{a}\frac{T^{1.5}}{D_*^{0.3}}$ $D_* = D_s\left(\frac{gR}{\nu^2}\right)^{1/3}$ $T = \frac{\tau_s^* - \tau_c^*}{\tau_c^*}$	if Δ known $\Delta/2$ else $a = k_s$ $a = \min(0.01H)$	Uniform
Akiyama and Fukushima (1986)	$E_s = 0 \quad Z < Z_c$ $E_s = 3\times 10^{-12}Z^{10}(1 - Z_c/Z) \quad Z_c < Z < Z_m$ $E_s = 0.3 \quad Z > Z_m$ $Z = \frac{u_s^*}{v_s}Re_p^{0.5}$	$a = 0.05H$	Uniform
Garcia and Parker (1991, 1993)	$E_{si} = \frac{A(\lambda Z_{ui})^5}{1+\frac{A}{0.3}(\lambda Z_{ui})^5}, \lambda = 1 - 0.288\sigma_\Phi$ $A = 1.3\times 10^{-7}$ $Z_{ui} = \frac{u_s^*}{v_{si}}f_1(R_{epi})\left(\frac{D_i}{D_g}\right)^{0.2}$ if $R_{epi} < 3.0$ then $f_1(R_{epi}) = 0.586R_{epi}^{1.23}$ else $f_1(R_{epi}) = R_{epi}^{0.6}$	$a = 0.05H$	Mixtures Uniform: $F_i = 1, \sigma_\Phi = 0$ $D_i/D_g = 1$
McLean (1991)	$E_{si} = \frac{0.65\gamma_0 S_0}{1+\gamma_0 S_0}\frac{\varphi_i F_i}{\sum_{n=1}^{N}\varphi_i F_i}$ $S_0 = \frac{\tau_s^* - \sqrt{\tau_c/\rho}}{\sqrt{\tau_{*c}/\rho}}, \gamma_0 = 0.004$ $\varphi_i = 1$ when $u_* > v_{si}$ otherwise $\varphi = \frac{u_* - u_{*cr}}{v_{si} - u_{*cr}}$	—	Mixtures
Zyserman and Fredsoe (1994)	$E_s = \frac{0.331A}{1+\frac{0.331}{0.46}A}, A = (\tau_s^* - 0.045)^{1.75}$	$a = 2D_s$	Uniform
Wright and Parker (2005)	$E_{si} = \frac{A(\lambda Z_{ui})^5}{1+\frac{A}{0.3}(\lambda Z_{ui})^5}, \lambda = 1 - 0.288\sigma_\Phi$ $A = 7.8\times 10^{-7}$ $Z_{ui} = \frac{u_s^*}{v_{si}}R_{epi}^{0.6}\left(\frac{D_i}{D_g}\right)^{0.2}S^{0.08}$	$a = 0.05H$	Mixtures Uniform: $F_i = 1, \sigma_\Phi = 0$ $D_i/D_g = 1$
Two-parameter model De Leeuw et al. (2020)	$E_{si} = \frac{Z_{ui}}{1+3Z_{ui}}$ $Z_{ui} = 4.74\times 10^{-4}\left(\left(\frac{u_s^*}{v_{si}}\right)^{1.5}Fr - 0.015\right)^{1.18}$ $Fr = \frac{U}{\sqrt{(gH_d)}}$	$a = 0.1H$	Mixtures

The first set of parameters (Π_1) in Eq. (7) denotes a ratio between the turbulent shear stress and gravitational forces. The second set (Π_2) relates the properties of the particle and the fluid. The third set (Π_3) has been proposed to quantify the hiding effect of the particles in mixture materials (Garcia and Parker 1991; Wright and Parker 2005), and some authors use the last set (Π_4) to include the hydraulic dimensionless parameters in the analysis (Wright and Parker 2005; De Leeuw et al. 2020).

The total bed shear stress, τ_b, exerted on a channel's bottom can be estimated via the one-dimensional (1D) momentum conservation equation for steady and uniform flow

$$\tau_b = \rho g R_h S \tag{9}$$

where τ_b = bed shear stress; ρ = water density; g = acceleration of gravity; R_h = hydraulic radius; and S = longitudinal energy slope. However, in the presence of bedforms, the concept of the bed shear stress partition is generally used to estimate the bed shear stress due to skin friction (τ_{bs}) and the bed shear stress associated with form drag (τ_{bf}) during the emergence of bedforms. Multiple formulations (Table 3) have been proposed in the literature to estimate τ_{bf} as a function of bedform type and its features. Smith and McLean (1977), Nelson and Smith (1989), and Fredsøe and Deigaard (1992) proposed formulations to determine the shear bed partition in the presence of dunes as a function of their wavelength and height, while Garcia and Parker (1993) proposed a formulation that can be used when ripples develop, and viscous effects are dominant.

Table 3. Formulations to estimate the drag component of the bed shear stress

Authors	Equations
Nelson and Smith (1989)	$\tau_{bf} = \frac{1}{2}\rho C_D \frac{\Delta_l}{\lambda_l} U_r^2$
	$\frac{U_r}{\sqrt{\tau_s/\rho}} = \frac{1}{\kappa}\left[\ln\left(30\frac{\Delta_l}{k_s}\right) - 1\right]$
Carnot's Formula Fredsøe and Deigaard (1992)	$\tau_{bf} = \frac{1}{2}\frac{U^2}{RgD}\frac{\Delta_l}{H}\frac{\Delta_l}{\lambda_l}$
Garcia and Parker (1993)	$\tau_{bf} = \frac{1}{2}C_D \frac{\Delta_l}{\lambda_l \kappa}\left[\ln\left[9\frac{u_s^* \Delta_l}{\nu}\right] - 1\right]^2 \rho U^2$

Methods

Entrainment Experiments

Annular Flume

A set of experiments were conducted in an annular flume located in the Ecohydraulics and Ecomorphodynamics Laboratory (EEL), at the University of Illinois (Fig. 1). This flume consists of a steel frame that supports a ring-shape annular fiberglass tank and two motor controllers that allow the tank and its plexiglass lid to rotate independently (the maximum angular velocities are 16.5 RPM and 10 RPM for the lid and the channel, respectively). The inner cross section of the annular tanks is a 20-cm-wide by 45-cm-deep channel whose depth can be modified by setting the lid height. The selection of this flume is based on (1) the relatively small amount of sample material needed to perform the experiments; (2) the experience with previous studies conducted with this flume with a fixed bed, with cohesive sediments and with iron ore tailings (UIUC and MWRDGC 2003; Pedocchi 2005; UIUC 2005; San Juan 2016); and (3) the potential formation of aggregates or flocs that could take place but would be preserved since no hydraulic machinery is required to generate the fluid motion.

Bed Shear Stress Characterization

To mimic an endless channel flow inside the annular flume, two main conditions were required: the minimization of secondary currents and the uniformity of the bed shear stress (τ_b) along the cross section. The first condition was achieved by counter-rotating the lid and the flume at a ratio Ω_L/Ω_C (where Ω_L and Ω_C are the angular velocities of the ring and flume, respectively) as discussed by Partheniades et al. (1966) and Petersen and Krishnappan (1994). The second condition relied on the near-bed instantaneous velocities along the cross section (Yang et al. 2000). According to Booij (1994) and Cantero et al. (2004), the optimum ratio is dependent on the specific objective of the experiment—erosion or deposition. The uniformity in τ_b is the primary requirement for erosion experiments, where the ratio Ω_L/Ω_c is not a sensitive criterion, and, consequently, a wide range of these ratios fulfill the uniformity of τ_b in the radial direction.

The experimental procedure aimed to find a ratio Ω_L/Ω_C that considerably minimized the secondary currents and, simultaneously, guaranteed a relatively uniform τ_b along the radial direction. The minimization of the secondary conditions was first achieved, and then the optimized ratio was slightly modified to achieve a relatively uniform τ_b in the radial direction. Mehta (1973) demonstrated that the previous condition is achieved when sediments tend to accumulate at the center of the channel (i.e., high sediment elevation in the outer wall implies a low Ω_L/Ω_C, and the opposite condition occurs when the sediment accumulates along the inner wall). Thus, multiple ratios Ω_L/Ω_C were tested using crushed walnut shells since they are easily movable under low shear stress conditions as their specific gravity is lower than that of sand (specific gravity of walnut shells, $S_{gr} = 1.48$). This relatively uniform walnut shell material ($D_m = 0.84$ mm to 1.0 mm) was placed

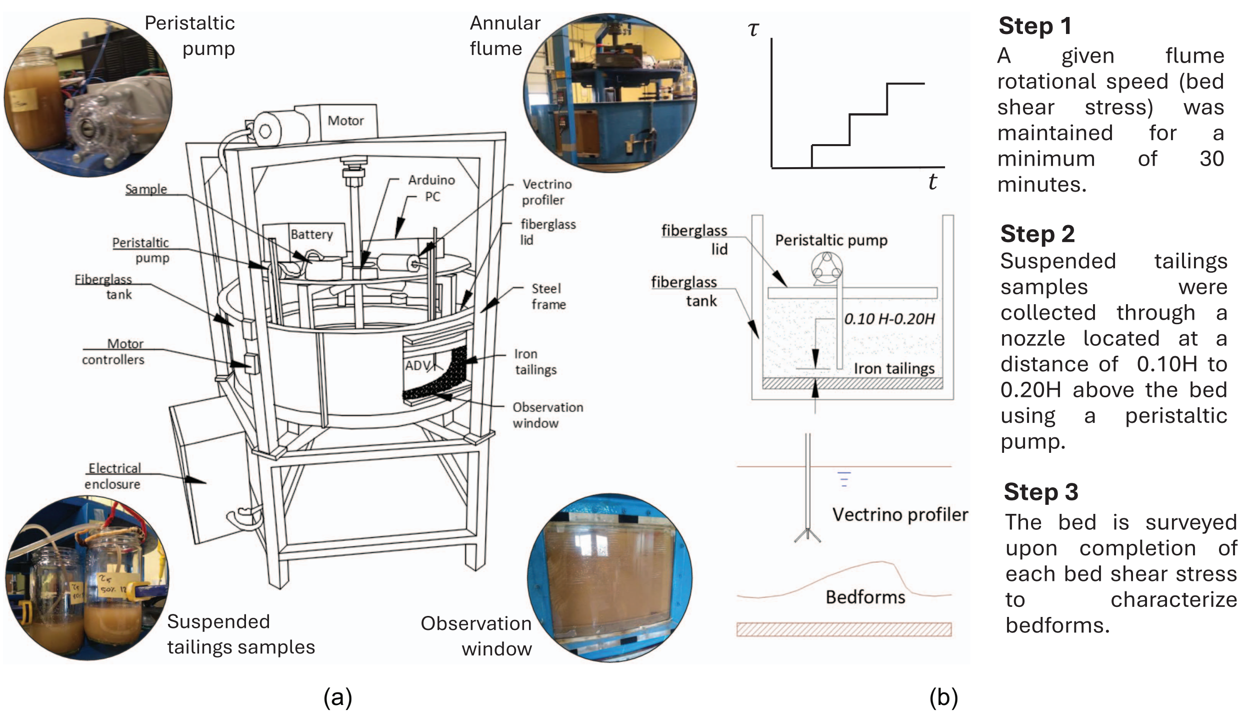

Fig. 1. (Color) (a) Schematic representation of the annular flume located at the EEL at the University of Illinois (data from San Juan 2016); and (b) steps followed during the sampling process in the entrainment experiment.

in a 10-cm-thick layer and flattened before testing the Ω_L/Ω ratios. To expedite this process, we also dumped 20 styrene spheres with a low density (specific gravity of styrene, $S_{gr} = 1.04$) to visually determine their position for different Ω_L/Ω_C ratios.

The velocity fluctuations time series were obtained employing Reynolds decomposition, and the bed shear stress τ_b was estimated via the turbulent kinetic energy (TKE) method

$$\tau_b = C_3 TKE = C_3 \frac{1}{2}\rho(\overline{u'^2} + \overline{v'^2} + \overline{w'^2}) \tag{10}$$

where u', v', and w' = fluctuations in the tangential, radial, and vertical directions, respectively (the bar over these variables denotes mean value); and C_3 is a dimensionless constant whose magnitude is in the range between 0.18 to 0.20 (Soulsby 1983). Herein, we adopted $C_3 = 0.19$ as it has proven to be valid for a wide range of flow conditions, and it has been previously used in annular flumes experiments (Thompson et al. 2003; Pope et al. 2006; Wei et al. 2017). The TKE method was chosen because of the unfeasibility of completely eliminating secondary currents in this annular flume. Thompson et al. (2003) and Pope et al. (2006) demonstrated that for movable beds in annular flumes, the TKE approach is more reliable than other proxy methods (e.g., Law of the Wall, Reynolds stresses, the Quadratic Stress Law).

To estimate the distribution of τ_b in the spanwise direction, the instantaneous velocities were measured at three different radii using a high-resolution acoustic doppler velocimetry (ADV) (Nortek Vectrino, Norway) mounted on the lid. This device was connected to a computer mounted on top of the lid. It was powered by a 12V battery and an AC/DC inverter and is controlled remotely via a wireless signal. The instantaneous velocities were measured in a time frame that guaranteed the convergence of the mean velocity at a sampling rate of 100 Hz. For the iron tailings placed on the annular flume, four minutes was sufficient to ensure the convergence of the mean values within 10% of the confidence interval.

Based on the previous methodology, we found that there are multiple ratios Ω_L/Ω_C that guarantee a quasi-uniform τ_b distribution along the spanwise direction. In this case, we selected $\Omega_L/\Omega_C = 2.75$ as it was also found in the analysis performed by Cantero et al. (2004) conducted with the same annular flume. A detailed analysis of the bed shear stress characterization can be found in Appendix I.

Multiple studies using annular flumes (Petersen and Krishnappan 1994; Partheniades et al. 1966; Cantero et al. 2004; Pedocchi 2005) have demonstrated that τ_b can be related to the quadratic velocity difference between the tangential velocities of the lid and the flume

$$\tau_b = \rho C_f \Delta U_{FL}^2 \tag{11}$$

where C_f = friction coefficient; and ΔU_{FL} = velocity difference between the lid and the flume. Based on the bed shear stresses τ_b [estimated via Eq. (10)] and the velocities of the lid and flume, it is possible to determine the friction coefficients C_f under different roughness conditions (the estimation of the roughness coefficients for the different samples tested in this study is presented in Appendix II).

The emergence of bedforms implies the partition of τ_b in two components—the particle skin friction and the form drag associated with the bedforms. As the former one is responsible for the sediment transport (Garcia 2008), the effect of the drag form was removed from the total shear stress as a way to estimate the bed shear stress associated with the skin friction (τ_{bs}). For dunes, we applied the Nelson-Smith partition (Table 3) to estimate the form drag component by characterizing the geometry of the bedforms (amplitude and wavelength). In the case of ripples, the equation derived by Garcia and Parker (1993) was implemented to estimate the τ_{bf} (Table 3).

Sample Preparation

Two iron ore tailing samples (S1 and S2) were prepared and tested under the same shear stress conditions to study the entrainment process for tailings. We also included information from previous experiments in which erosion analysis was conducted for an iron tailings sample (S3). A simple soil characterization was performed for Samples S1 and S2, including granular size distribution [GSD, Fig. 2(a)], and specific gravity per fraction [Fig. 2(b)] according to the standards ASTM D854-14 (ASTM 2014), ASTM D7928 (ASTM 2017a), and ASTM D6913 (ASTM 2017b). The mineralogical composition of Samples S1 and S2 showed that silica was the main mineral with weight fractions above 50%. The percentage of fine fractions ($D < 62.5$ μm) are 21.0%, 46.9%, and 40.6% for Samples S1, S2, and S3, respectively.

Experimental Procedure and Data Collection

To guarantee a well-mixed bed and to avoid any grading in the bed, each sample was well-mixed by means of a cement mixer and then

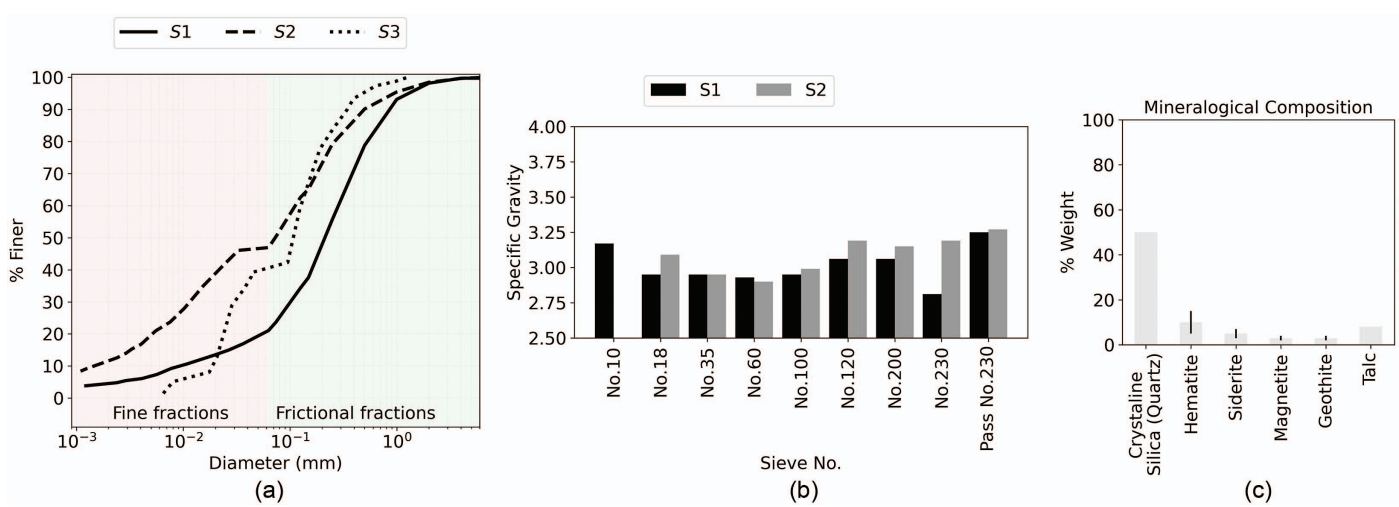

Fig. 2. (Color) (a) Granular size distribution for Samples S1, S2, and S3; (b) specific gravity per fraction for Samples S1 and S2; and (c) mineralogical composition for Samples S1 and S2.

was placed in the annular flume in a 10-cm layer that was uniformly leveled. The 25-cm water depth (H) was filled slowly to minimize any considerable resuspension along the water column. Thereafter, the flume was allowed to sit for 7 days. Geremew and Yanful (2011) reported that at least 36 h are required to resemble the natural settling and consolidation in pounded water.

Based on the shear stress characterization, we performed the erosion test for different values of rotational speeds, starting by spinning the lid and the flume with a slow rotational speed (i.e., a relatively low bed shear stress). For each sample, eight different shear stresses were selected and increased step-wise. For each shear stress, the flume was allowed to turn at a constant speed for a minimum of 30 min to guarantee equilibrium conditions.

Near-bed tailings samples were taken in a sampling port set at 10% of the total water depth ($0.10H$). When dunes emerged, the sampling port was moved to around $0.20H$ to prevent any obstruction of sampling tube. These samples were extracted employing a peristaltic pump to minimize the alteration of the sediment structures (e.g., flocs). This pump was controlled by a microcontroller board (ARDUINO UNO, Arduino, Scarmagno, Italy) operated via a wireless connection. The microcontroller and the pump mounted to the flume lid extracted an approximately 800-mL sample of the suspended sediment mixture. To avoid bias in the subsequent samples, the peristaltic pump was reversed, and the hose was filled with clean water right after extraction. Also, clean water was added to the flume to replace the amount of water extracted from the flume during sampling. The near-bed suspended sediment concentration (C_a) was then determined according to ASTM D3977-97 (ASTM 2019).

After extracting the sediment sample, a survey along the centerline was conducted to determine the presence of bedforms. An acoustic doppler vectrino profiler (ADV-II) (Nortek) was mounted on the lid of the annular flume to survey the centerline at 1 Hz to characterize the geometry of the dunes (amplitude and wavelength). To avoid any alteration of the bedforms, we fixed the lid and gradually decreased the flume's angular velocity until it reached 0.5 RPM. For high bed shear stress values (i.e., high suspended sediment concentrations), we let the sediment sit until the ADV measurements were reliable. These measurements were taken upon completing each combination of rotational speeds (i.e., Ω_L/Ω_C ratios).

To determine the GSD of the suspended samples, we used a Malvern 3000 (Malvern Panalytical, Worcestershire, UK) particle sizer. The volume extracted from the sample was diluted in 500 mL of deionized water until the solution reached an obscuration value between 10% to 20%. We extracted this volume by using a pipette, while the sample was mixed thoroughly with a plastic stirrer (we avoided the use of a magnetic stirrer as the sample had a high content of iron).

Flocculation and Hindered Settling Experiments

Settling column tests were conducted to determine whether or not flocculation and hindered settling could be relevant for the materials tested in the annular flume experiments. We followed the experimental approach proposed by Ross (1988) in which a settling column, with taps positioned at different heights (0.06, 0.16, 0.31, 0.51, 0.72, 0.93, 1.13, and 1.54 m), is used to determine the concentration profile evolution of an initial uniform concentration under quiescent water conditions.

During the experiment, we considered four different concentrations of suspended tailings (4 g/L, 16 g/L, 26 g/L, and 40 g/L) obtained from the reconstituted Sample S2. This analysis exclusively considers particles with diameters below 62.5 μm, which were obtained by means of the sieving method (sieve no. 230). The suspended tailings samples were taken simultaneously through the nine 5-mm sampling taps at different times (1, 5, 10, 15, 30, 60, 120, and 180 min). For a detailed description of the experimental setup and the procedures, please refer to works by Ross (1988), Hwang and Mehta (1989), and Fernández et al. (2018).

The occurrence of the hindered settling and flocculation is assessed based on the methods outlined by McLaughlin (1958, 1959) and presented in Vanoni (2006). These methods are based on concentration profiles and the continuity equation for a suspension settling in quiescent water. This fundamental sediment mass balance equation is

$$\frac{\partial C}{\partial t} + \frac{\partial v_s C}{\partial z} = 0 \tag{12}$$

where C = total particle concentration; v_s = sediment fall velocity; t = time; and z = vertical distance from the bottom.

Results

Bedform Characterization

The development of bedforms was captured by measuring the centerline for larger τ_b. [Fig. 3(a)]. Fig. 3(b) depicts the dimensionless total bed shear stress that is accounted for by skin friction and bedform drag. The vertical distance between the τ_b^* (x-axis) and each curve represents the magnitude of the τ_{bs}^* for each sample; while the distance between these curves and the 45° line defines the amount of the total shear stress that is lost to form drag. The majority of the total shear stress acts on the bed as skin friction for low values of τ_b^* (prior to the development of the large bedforms). As the bedforms develop, the form drag increases and the percentage of the total shear stress that is attributable to skin friction decreases.

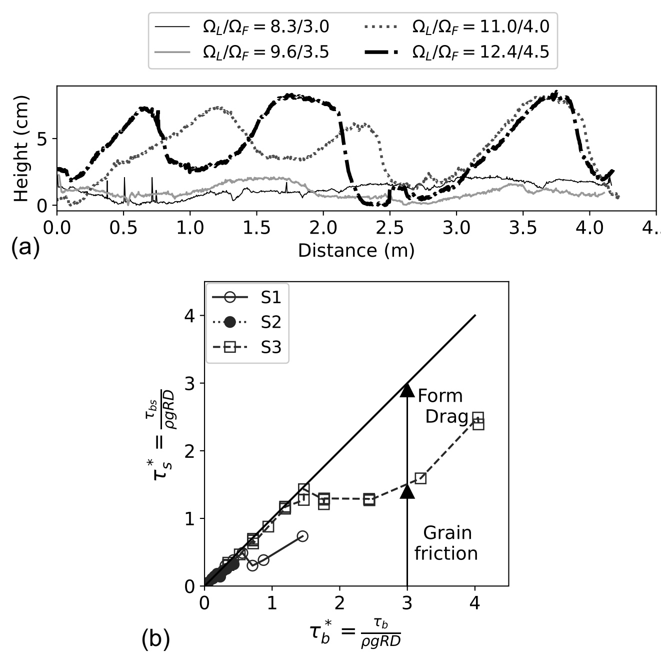

Fig. 3. (a) Dunes measured for some Ω_L/Ω_C ratios for Sample S1; and (b) dimensionless skin friction τ_{bs}^* as a function of total bed Shields number τ_b.

Cohesion, Flocculation, and Hindered Settling

Although all three samples had $\phi_{fines} < 50\%$, we aim to determine whether the erosion rate of the tailings samples followed the cohesive relation derived for natural cohesive materials [Eq. (1)]. As Sample S2 has the highest content of fines, we performed a curve-fitting to establish the magnitudes of α and θ. Although τ_{cr} oscillate in a range between 0.09 and 0.2 Pa, we chose $\tau_{cr} = 0.09$ Pa to the intersection of a linear trendline with the x-axis for the scatter plot E versus τ_b (Fig. 4). The correlation coefficient ($R^2 = 0.57$) suggests that the fines content is insufficient to classify this material as cohesive. Previous studies have shown that $R^2 > 0.86$ are indicative of cohesive tailings (Geremew and Yanful 2011).

To evaluate the occurrence of flocculation and hindered setting processes of the tailings, Fig. 5 depicts the spatiotemporal evolution of the normalized concentration profiles based on the initial concentrations, C_o, (dots and solid lines). The general trend of these profiles is that the concentrations along the water column decrease

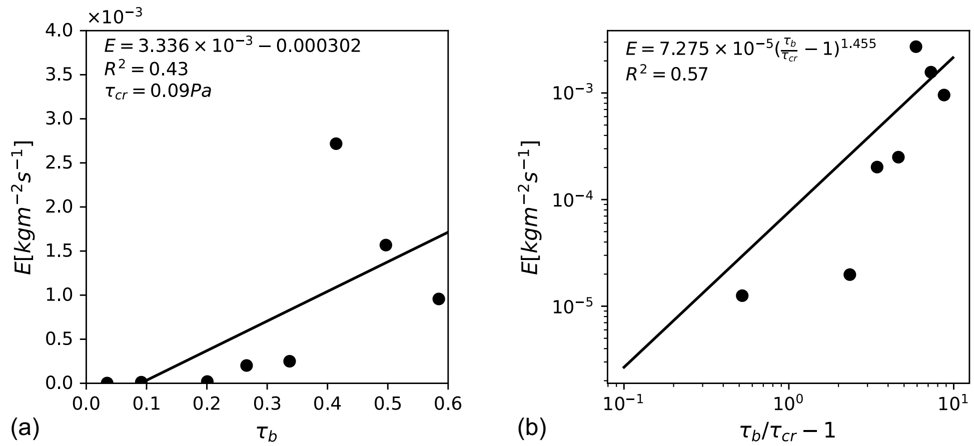

Fig. 4. (a) Critical shear stress estimation for the fine material assuming a cohesive behavior; and (b) relation between excess of shear stress and erosion for fine tailings (S2).

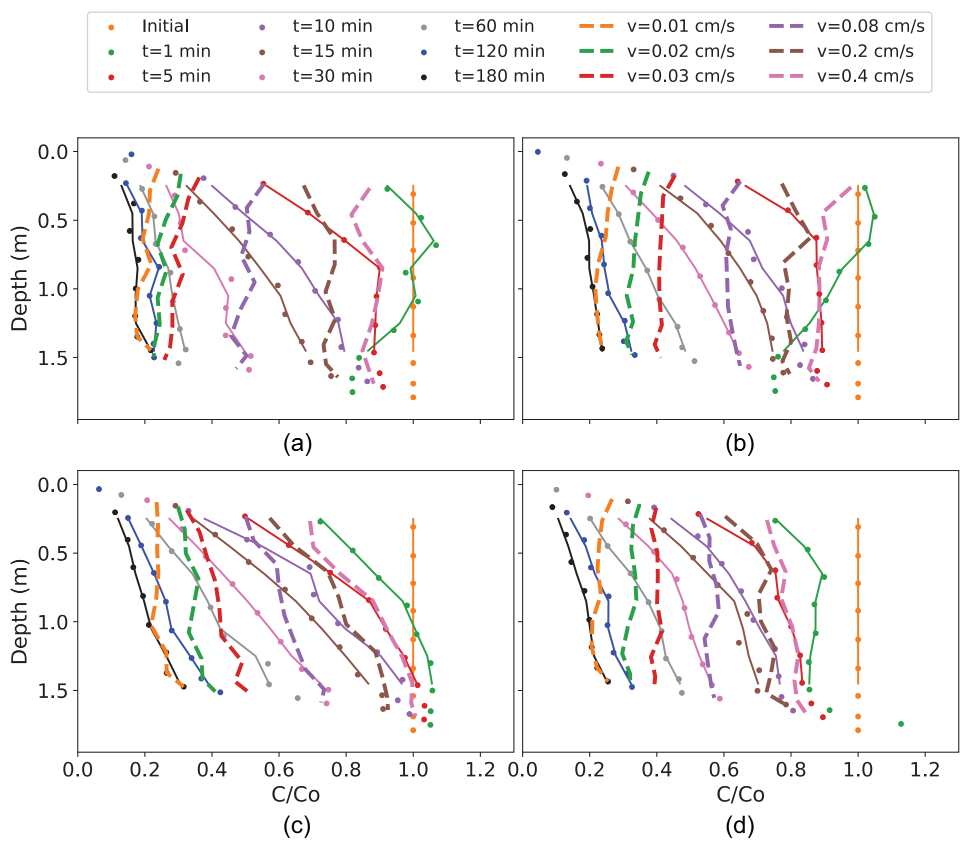

Fig. 5. (Color) Concentration profiles (solid lines and dots) and different free settling velocities (dashed lines). The dots represent the concentration measurements at different depths and times, and the solid lines show the evolution of the concentration profiles at fixed depths: (a) $C_0 = 4$ g/L; (b) $C_0 = 16$ g/L; (c) $C_0 = 26$ g/L; and (d) $C_0 = 40$ g/L.

over time, as the sediment settles down to the bottom. However, for certain initial concentrations C_o, a sudden concentration increase is observed at different depths during the first minutes (i.e., $t = 1$ min) of the experimental test.

The dashed lines in Fig. 5 represent the concentrations measured by an observer descending at a constant velocity along the water column. The dashed lines have a parallel trend with respect to the y-axis, indicating that neither flocculation nor hindered settling processes dominate. These observations are seen when the experiments are conducted with both tap and distilled water. There is a sign of hindered processes occurring for the initial times t for the test with $C_o = 26$ g/L as the dashed lines are sloping away from the y-axis. However, this phenomenon is not considered as relevant as it was not found to be significant for the tests with higher concentrations (i.e., $C_o = 40$ g/L).

Near-Bed Suspended Tailings Concentration

Uniform Bed Distribution

For the assumption of a uniform bed distribution, we use the D_{50} as a representative diameter to compare the performance of the existing entrainment formulations as predictors of the near-bed concentrations measured during the experiments (Table 2). After finding that flocculation and hindered processes were irrelevant, we estimated the free settling velocity via Eq. (8). For the tested iron tailings samples (S1 and S2), we assigned $C_1 = 20$ and $C_2 = 1.1$ as these materials have an important content of silica (Fig. 2). As some of the concentration samples were taken at different heights due to the emergence of the bedforms, the near-bed suspended tailings concentration for different reference heights a were estimated assuming that distribution of the suspended sediment follows Rouse's equilibrium profile [Eq. (5)]. To account for the effects of sediment stratification due to the high sediment concentrations, we assign $\beta = 0.94$ based on the analysis conducted by De Leeuw et al. (2020). To assess the entrainment formulation proposed by Wright and Parker (2005), we assumed that equilibrium and uniform flow conditions are achieved at each τ_b, thus, friction slope was determined via Eq. (9).

The assessment of the performance of the entrainment relations with the measured data was conducted by comparing the observed entrainment $E_{s-obs} = f_{ai}C_{ai}/F_i$ ($f_{ai}/F_i = 1$ for uniform bed distribution assumption) versus the predicted values estimated via the entrainment formulations (Fig. 6). We use the mean discrepancy ratio M_e

$$M_e = 10^{b_1}, \qquad b_1 = \frac{1}{n_o}\sum_{n=1}^{n_o} \log\left(\frac{E_{s-pred}}{E_{s-obs}}\right) \tag{13}$$

the mean absolute mean discrepancy ratio A_d

$$A_d = 10^{b_2}, \qquad b_2 = \frac{1}{n_o}\left|\sum_{n=1}^{n_o} \log\left(\frac{E_{s-pred}}{E_{s-obs}}\right) - b_1\right| \tag{14}$$

and the residual sum of squares, RSS [Eq. (15)]

$$RSS = \sum_{n=1}^{n_o} (\ln(E_{s-pred}) - \ln(E_{s-obs}))^2 \tag{15}$$

where n_0 = number of data points; and E_{s-pred} and E_{s-obs} = predicted and observed entrainment, respectively. The performance of these entrainment formulations are presented in Table 4.

The assessment of the predicted entrainment rates shows that there is no universal formulation able to predict the observed data. The formulations tend to better predict the values for Sample S1, followed by S3 and then by S2, as these equations were developed for sand-size material.

Among the seven relations assessed in this analysis, the Garcia and Parker (1991) complemented by Garcia and Parker (1993) formulations give the best predictions overall as M_e and A_d values are closer to 1.0 and RSS values are relatively low for all samples (Table 4). Also, a suitable collapse of the data of all samples can be observed when the dimensionless parameter Z_u is plotted against the observed dimensionless entrainment rate [Fig. 7(b)]. This provides evidence that there is a clear dependence of the entrainment or near-bed volumetric sediment concentration values with the dimensionless shear velocity parameter u_s^*/v_s, since the value of

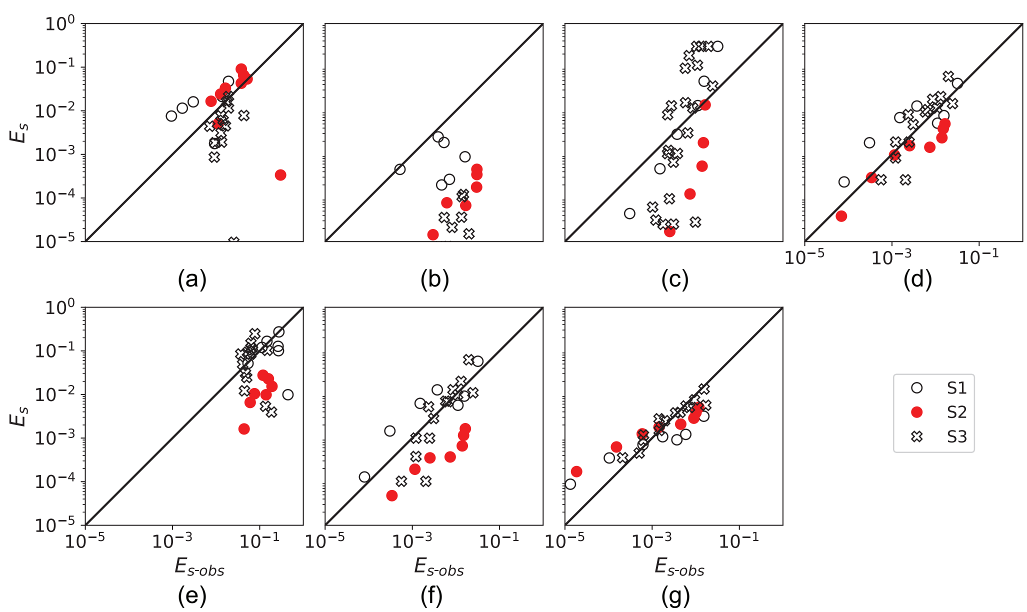

Fig. 6. (Color) Observed and predicted entrainment comparison: (a) Smith and McLean (1977); (b) van Rijn (1984); (c) Akiyama and Fukushima (1986); (d) Garcia and Parker (1991, 1993); (e) Zyserman and Fredsoe (1994); (f) Wright and Parker (2005); and (g) De Leeuw et al. (2020).

Table 4. Performance of the entrainment equations

Equation	S1			S2			S3		
	M_e	A_d	RSS	M_e	A_d	RSS	M_e	A_d	RSS
1. Smith and McLean (1977)	5.44	6.58	14.84	0.36	30.74	49.27	0.17	3.7	82.25
2. van Rijn (1984)	0.04	9.25	30.54	0.0	11.89	141.97	0.02	16.57	279.11
3. Akiyama and Fukushima (1986)	1.05	7.27	11.5	0.02	11.03	56.8	0.33	125.99	200.3
4. Garcia and Parker (1991)	7.31	8.73	15.39	0.08	4.67	16.25	1.14	2.21	9.81
5. Zyserman and Fredsoe (1994)	0.01	699.87	157.42	0.02	2.94	39.03	0.66	3.67	31.67
6. Wright and Parker (2005)	4.84	5.24	9.26	0.0	4.69	74.62	0.65	2.55	17.14
7. De Leeuw et al. (2020)	3.12	69.93	45.48	2.36	15.78	17.37	1.03	1.49	2.71

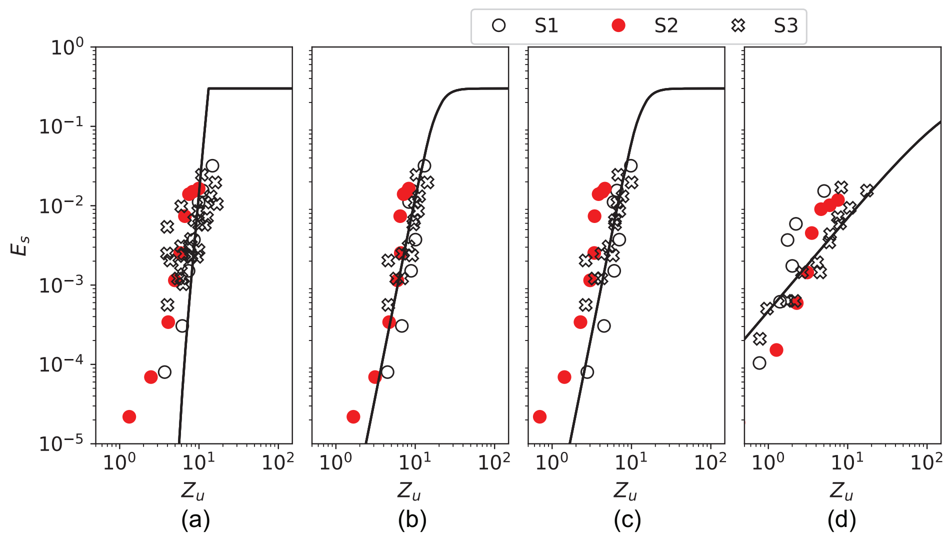

Fig. 7. (Color) The values of Z_u versus E_s for uniform bed distribution: (a) Akiyama and Fukushima (1986); (b) Garcia and Parker (1991); (c) Wright and Parker (2005); and (d) De Leeuw et al. (2020).

R_{ep} is almost constant for each material (as D_{50} and R are constant, and ν is a function of the water temperature).

Mixtures

For the analysis of mixtures we assessed the formulations proposed by Garcia and Parker (1991), Wright and Parker (2005), and De Leeuw et al. (2020) as they have the best performance on predicting the entrainment of the iron tailings for uniform bed conditions (Table 4 and Fig. 7). For this analysis, we used the entrainment results from Samples S1 and S2, since the suspended tailings fractions were determined during these experiments.

The formulations proposed by Garcia and Parker (1991) and Wright and Parker (2005) were used to assess the E_{si} based on the lumped dimensionless parameters represented in the similarity variable Z_{ui} [Figs. 8(a and b)]. Although there is a clear dependence of E_{si} with Z_{ui} ($E_{si} \sim Z_{ui}^8$), a considerable scatter is seen in both formulations when the function f_1 (if $R_{epi} < 3.0$ then $f_1(R_{epi}) = 0.586R_{epi}^{1.23}$ else $f_1(R_{epi}) = R_{epi}^{0.6}$) proposed by Garcia and Parker (1993) is not included in the similarity function, Z_{ui}. The inclusion of this function leads to an independent and parallel collapse of samples S1 and S2 as depicted in Figs. 8(c and d). Despite this collapse, these two formulations underestimate the entrainment for all fractions in sample S2, but tend to reasonably predict the entrainment for the coarse sample S1. It is important to emphasize that despite the fairly good collapse, the slope of both samples differs slightly from the slope of the $E_s - \lambda Z_u$ curve.

The independent collapse of Samples S1 and S2 depicted in Figs. 8(c and d) reveals the pertinence of involving an inherent property of the material in the similarity variable. After some iterations, we found that both samples collapse when the inverse of the relative roughness H/k_c (k_c is the composite roughness that considers the effect of both the grain friction and form drag) is added to the original formulations (Garcia 2008). Herein, we selected C_f, as this dimensionless parameter involves the term H/k_c in its formulation. For instance, the Keulegan's resistance law is given by

$$\frac{1}{C_f} = \frac{U}{\sqrt{\tau_{bs} + \tau_{bf}}} = \frac{1}{\kappa}\ln\left(11\frac{H}{k_c}\right) \quad (16)$$

Therefore, this finding indicates that the near-bed tailings concentration for mixtures depends on the dimensionless parameters outlined in the following:

$$E_{si} = f\left(\frac{u_s^*}{v_{si}}, R_{epi}, \frac{D_i}{D_g}, S, C_f\right) \quad (17)$$

Keeping the same formulation structure proposed by Garcia and Parker (1991) and Wright and Parker (2005), the similarity variable Z_{ui} can be written as follows:

$$Z_{ui} = \frac{u_s^*}{v_{si}} f_1(R_{epi}) \left(\frac{D_i}{D_g}\right)^{0.2} S^n f_2(C_f) \quad (18)$$

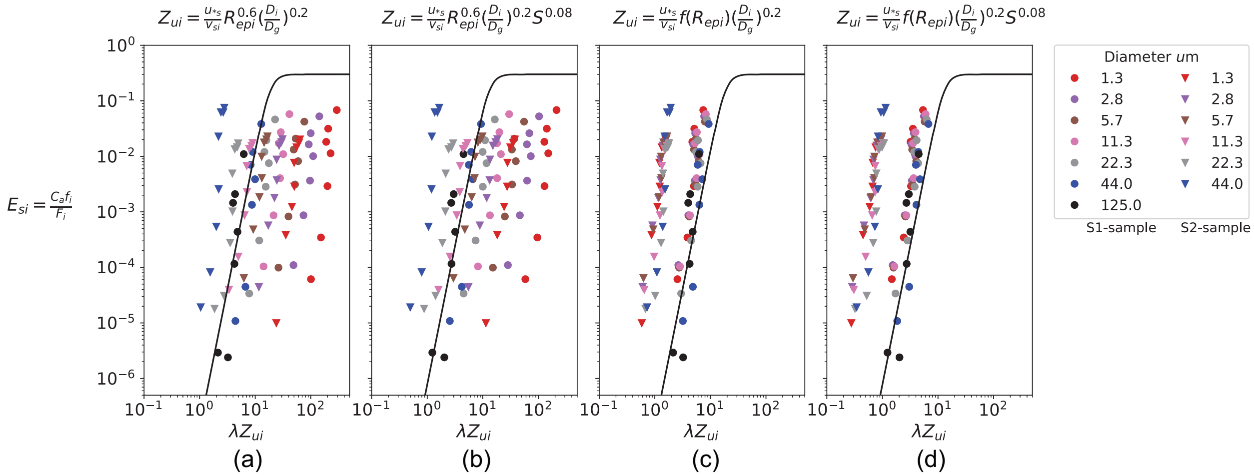

Fig. 8. (Color) The values of Z_u versus E_s for mixtures for S1 and S2 samples: (a) Garcia and Parker (1991); (b) Wright and Parker (2005); (c) Garcia and Parker (1991) complemented by Garcia and Parker (1993) for $R_{epi} < 3.0$; and (d) Wright and Parker (2005) complemented by Garcia and Parker (1993) for $R_{epi} < 3.0$.

where f_1 and f_2 = power functions; and n is an exponent equal to 0 or 0.08 for the formulations proposed by Garcia and Parker (1991) and Wright and Parker (2005), respectively.

The involvement of function f_1 in this analysis collapses the data as it includes the dimensionless parameter R_{epi}, which implicitly accounts for the ratio of the viscous sublayer thickness and the particle sizes. This parameter is essential herein as the particle sizes measured in the suspended samples (S1 and S2) might be fully or partially immersed in the viscous sublayer. Although the f_1 function proposed by Garcia and Parker (1993) collapses the data, its development was performed based on entrainment experiments on two independent uniform-size samples of fine-crushed coal. To determine whether the f_1 function is suitable for tailings materials, we analyzed the size dependence when this function is included as part of the similarity variable Z_{ui}. By considering the definition of R_{epi} [Eq. (7*b*)], Eq. (18) can be rewritten as

$$Z_{ui} = \left[a_1 \frac{u_s^* (R_i g)^{0.3}}{\nu^{0.6} D_g^{0.2}} S^n C_f^p \right] \frac{D_i^m}{v_{si}} \qquad (19)$$

where m is an exponent equal to 0.9 for uniform material, 1.1 for mixtures with $R_{epi} > 3.0$ and 2.045 for $R_{epi} < 3.0$; p is an exponent that differs from zero in this study and zero for the original formulations; and a_1 is a constant that absorbs the scaling factors from functions f_1 and f_2.

Eq. (19) shows that $Z_{ui} \propto D_i^m / v_{si}$. The value of m mainly depends on the function f_1 followed by the dimensionless parameter associated with the hiding effect. The f_1 function proposed by Garcia and Parker (1991), denoted as $f_1 = R_{epi}^{0.6}$, leads to a decrease in Z_{ui} as the grain size increases [see green and magenta lines in Fig. 9(a)]. However, the modified f_1 function proposed by Garcia and Parker (1993) for $R_{ep} < 3.0$ (i.e., $f_1 = 0.586 R_{epi}^{1.23}$) exhibits slight increments in Z_{ui} when the grain size increases [see blue line in Fig. 9(a)].

We found that the best independent data collapse [Figs. 8(c and d)] is achieved when the exponent value in function $f_1(R_{epi})$ is equal to 1.16 instead of 1.23. This new exponent leads to a slight decrease of Z_{ui} (and therefore E_{si}) when the particle size increases [see black line in Fig. 9(a)]. The determination of the threshold for f_1, which distinguishes particles influenced and not influenced by the thickness of the viscous sublayer, involved multiple iterations to achieve a suitable collapse of all grain sizes [Figs. 8(c and d)]. We established that a reasonable threshold is $R_{epi} = 4.5$, slightly higher than the $R_{epi} = 3.0$ proposed earlier by Garcia and Parker (1993). To avoid a discontinuity in function $f_1(R_{epi})$ as seen in Garcia and Parker (1993) when $R_{epi} = 3.0$ [see blue line in Fig. 9(b)] and to satisfy the aforementioned threshold, we proposed a modified function such as $f_1 = 0.43 R_{epi}^{1.16}$.

The subsequent step is to define the function $f_2(C_f) = a_0 C_f^p$ to address the independent collapse seen in Figs. 8(c and d). By setting $p = -0.28$, we achieved the collapse of both samples in

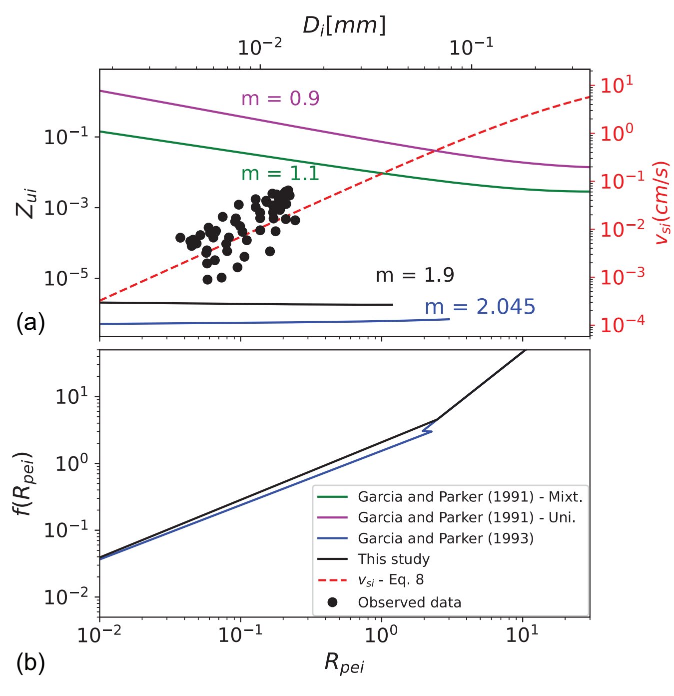

Fig. 9. (Color) (a) The values of Z_{ui} versus R_{epi} and v_{si} [Eq. (8), right y-axis], all the terms in brackets in Eq. (19) are set to unity; and (b) original $f_{R_{epi}}$ proposed by Garcia and Parker (1993) and the modification proposed herein. The observed data are estimated based on the evolution of the D_{50} of the suspended sediment samples taken during the settling column experiments with an initial concentration of $C_o = 16$ g/L.

all range sizes. The parameter a_0 was determined by fitting the collapsed data, assuming a unique representative diameter (i.e., D_g) for Samples S1 and S2. This fitting utilizes the uniform entrainment formulation [$E_s = AZ^\gamma/(1 + A/0.3Z^\gamma)$], and adjusts the original exponent $\gamma = 5$ to $\gamma = 8$ to match the slope of the collapsed data (as $E_{si} \sim Z_{ui}^8$). Based on the preceding analysis, the similarity variable Z_{ui} [Eq. (18)] is then redefined as

$$Z_{ui} = \frac{u_s^*}{v_{si}} f_1(R_{epi}) \left(\frac{D_i}{D_g}\right)^{0.2} f_2(C_f) S^n \qquad (20)$$

where

$$f_1(R_{epi}) = \begin{cases} R_{epi}^{0.6}, & \text{if } R_{epi} > 4.5 \\ 0.43 R_{epi}^{1.16}, & \text{otherwise} \end{cases}$$

$$f_2(C_f) = a_0 C_f^p, \qquad a_0 = 0.081, \qquad p = -0.28$$

where $n = 0.08$ if the energy slope is considered in this analysis (Wright and Parker 2005), or $n = 0$ otherwise (Garcia and Parker 1991).

The strained parameter λ was implemented to independently fit the collapsed data to the proposed entrainment formulation

$$E_{si} = \frac{A(\lambda Z_{ui})^8}{1 + \frac{A}{0.3}(\lambda Z_{ui})^8} \qquad (21)$$

where

$$A = \begin{cases} 1.3 \times 10^{-7}, & \text{if } n = 0 \\ 7.8 \times 10^{-6}, & \text{if } n = 0.08 \end{cases}$$

Following the approach by Garcia and Parker (1991), λ is determined based on the geometric standard deviation σ_φ ($\sigma_{S1} = 2.07$ and $\sigma_{S2} = 2.58$, $\lambda_{S1} = 0.76$, and $\lambda_{S2} = 1.26$) leading to $\lambda = 1 - 0.0038\sigma_\phi$. Fig. 10 depicts the collapsed data for both samples along with the $E_s - \lambda Z_u$ line based on Eq. (21). Likewise, the comparison between the observed and predicted entrainment based on the original formulations proposed by Garcia and Parker (1991) and Wright and Parker (2005), along with Eqs. (20) and (21) are shown in Fig. 11. The inclusion of the dimensionless parameter S slightly improves the collapse of the $E_{\text{sobs}-i}$ data, enhancing the prediction of the observed data [Figs. 11(d and e)].

We also evaluated a three-parameter model to predict E_{si} at $0.10H$ using the dimensionless parameters proposed by De Leeuw et al. (2020). However, instead of considering u^*/v_{si}, herein we selected u_s^*/v_{si} due to the presence of bedforms during the experiment

$$E_{si} = e_1(u_s^*/v_{si})^{e_2} Fr^{e_3} R_{epi}^{e_4} \qquad (22)$$

where $e_1 = 0.002$, $e_2 = 0.60$, $e_3 = 4.88$, and $e_4 = 0.40$ are parameters that are determined based on a best-fitting analysis.

The performance of the best-fit three-parameter model [Eq. (22)] is shown in Fig. 11(f) and compared with the formulation proposed by De Leeuw et al. (2020) [Fig. 11(c)]. Like the f_1 function described previously, the inclusion of R_{epi} in this three-parameter model is essential for collapsing the observed data. In this equation, hiding effects are not included, and the hydraulic dimensionless parameters C_f and H/k_c are instead represented by the Froude number, Fr (see analysis in the "Discussion" section).

To test the proposed Eqs. (20) and (21) (considering S), and Eq. (22), we used the information from Sample S3, as this data was not used in deriving the proposed formulation. The main drawback when using this data is that size fractions were not measured in the suspended samples. Therefore, herein, we treat this sample as well-sorted material as the proposed formulations can also be applied to this condition (i.e., $D_i/D_g = 1$ and $\sigma_\phi = 0$). Fig. 12 shows the comparison between the observed data and the formulation proposed herein assuming a unique representative diameter for the S3 sample (i.e., D_g). The comparison between the observed and predicted data shows a low performance of both equations in predicting the entrainment of the S3 material into the water column. One reason could be that D_g cannot be selected as a representative diameter as there is a high chance that the suspended samples contain fractions smaller than D_g. Therefore, we recommend performing similar experiments for future studies to adequately validate the formulations proposed in this study.

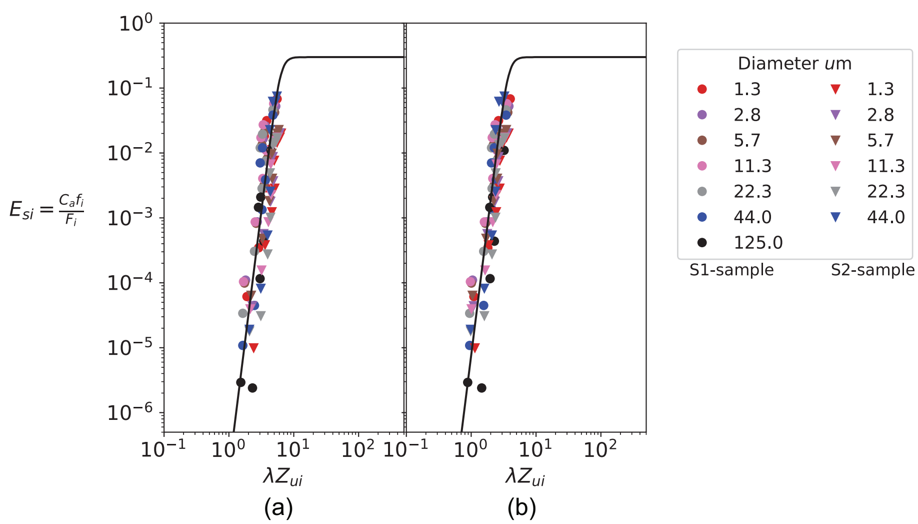

Fig. 10. (Color) The values of λZ_{ui} versus E_{si} for mixtures for S1 and S2 samples: (a) Eqs. (20) and (21) without considering S; and (b) Eqs. (20) and (21) considering S.

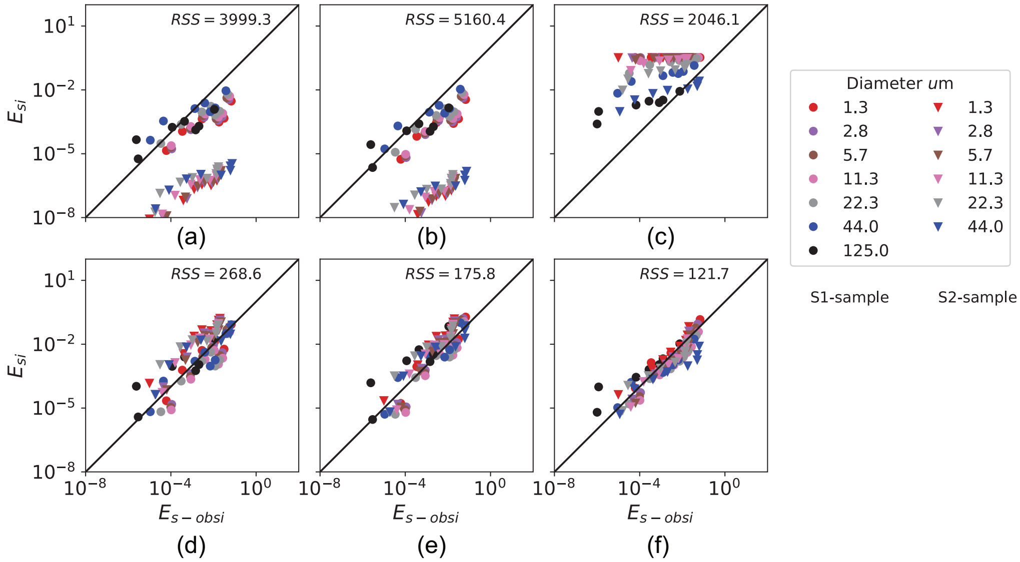

Fig. 11. (Color) The values of E_{si} versus $E_{\mathrm{sobs}-i}$ (a) Garcia and Parker (1991); (b) Wright and Parker (2005); (c) De Leeuw et al. (2020); (d) Eqs. (20) and (21) without considering S; (e) Eqs. (20) and (21) considering S; and (f) Eq. (22).

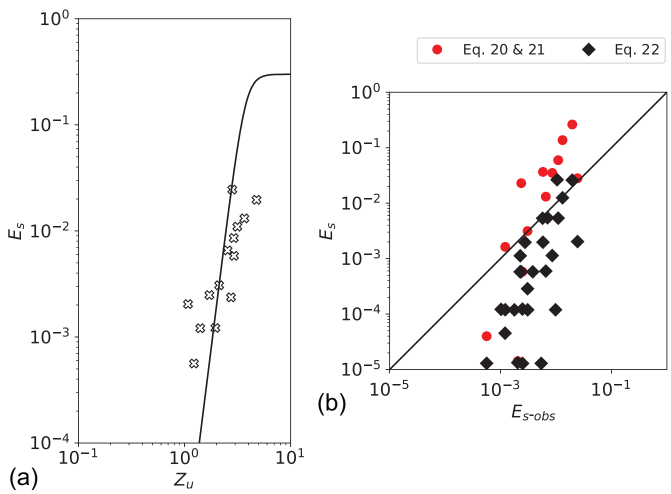

Fig. 12. (Color) Comparison between observed and predicted values treating S3 as a uniform sample: (a) Z_u versus E_s; and (b) E_{s-obs} versus E_s.

Discussion

Although the current research focuses on the entrainment of iron tailings, we expect that the proposed entrainment formulations are also applicable to noncohesive materials with sediment densities and grain size distributions similar to those of iron tailings tested in this study. The main difference between the proposed formulations and the original ones is the inclusion of functions f_1 and f_2 in the similarity variable. Consequently, it is relevant to discuss the importance of these two functions in the entrainment formulations.

Based on the results obtained, the inclusion of the relative roughness H/k_c (represented as C_f) is not only relevant for large sand-bed rivers but is also essential for predicting the entrainment in silt- and fine sand-rich bed streams. However, according to Fig. 8(d), this dimensionless parameter (and thus function f_2) might be a nonessential contributor for the entrainment prediction in sand-bed river conditions as the original formulations seem to reasonably predict the entrainment, despite the slope differences between the collapse of the coarse material and the entrainment formulation.

It might be redundant to include the energy slope S and the H/k_c (or C_f) in Z_{ui}, as Wright and Parker (2005) claim that both tend to be correlated. However, the current experimental analysis shows that these two dimensionless parameters complement each other. The f_2 involves the roughness of the material in the entrainment functions while the slope S contributes to collapsing the data around the $E_{si} - \lambda Z_{ui}$ curve and is more related to the stratification effects that might be occurring in the experiment due to the high suspended tailings concentrations.

On the other hand, the main purpose of function f_1 is to involve the particle-fluid interactions within the entrainment formulations. The importance of including the dimensionless parameter R_{epi} to predict E_{si} lies in the selected grain sizes. De Leeuw et al. (2020) showed that, in the case of sand-bed rivers with $D_i > 63$ μm, there is no significant improvement in the entrainment predictions if the dimensionless parameter R_{epi} is included in the formulations. However, herein we corroborate that for a silt-rich bed, particle-fluid interaction within the viscous sublayer plays an important role in the prediction of the entrainment, and hence, the inclusion of the dimensionless parameter R_{epi} is essential for small grain sizes (i.e., $D_i < 63$ μm).

The current analysis and the one conducted by Garcia and Parker (1993) demonstrate that the incorporation of $f_1(R_{epi})$ into Z_{ui} restricts the entrainment of bed material into the water column for low R_{epi} values (or small D_i). For the tailings mixtures analyzed in this research, we found that the combination of the hiding effects and the role of particle-fluid interaction leads to a slight increase in Z_{ui} with increasing R_{epi} [see green line in Fig. 9(b)]. Nevertheless, Z_{ui} slightly increases (and thus the entrainment E_{si}) with the diameter when Garcia and Parker (1993) function is considered. This behavior is compatible with experimental observations for uniform beds in which diameters immersed in the viscous sublayer require higher turbulent intensities than larger diameters that protrude from this sublayer (Nino et al. 2003).

Fig. 13 shows that most of the diameters measured in the suspended samples were immersed in the viscous sublayer ($\delta_v = 11.6\nu/u_*$). Therefore, the particle-fluid interaction plays

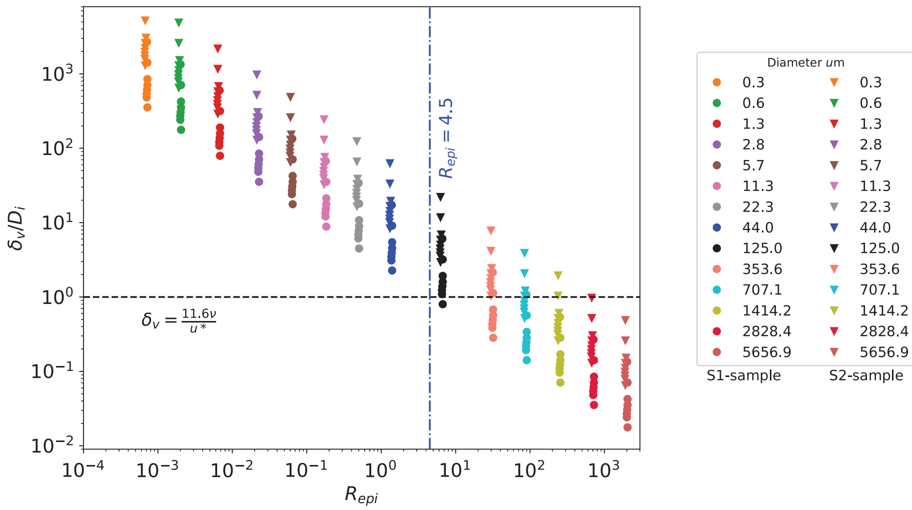

Fig. 13. (Color) Comparison between the thickness of the viscous sublayer ($\delta_v = 11.6\nu/u_*$) and the diameter (δ_v/D_i) versus R_{epi}.

an important role in the entrainment of particles up to diameters smaller than the thickness of this viscous sublayer (i.e., $D_i <$ 44 μm). The threshold where the diameters protrude from this sublayer coincides with the proposed threshold ($R_{epi} = 4.5$) found for the transition between the original $f_1 = R_{epi}^{0.6}$ (Garcia and Parker 1991) for open channel sediment and the one proposed in this work.

On the other hand, upon initial observation, the three-parameter equation [Eq. (22)] appears to be more parsimonious than Eq. (20) as the latter one requires five parameters to predict the E_{si}. However, one can demonstrate that for steady and uniform flow conditions, the Froude number Fr is related to the energy slope S and the friction coefficient C_f when Eqs. (9) and (11) are equated

$$Fr^2 = \frac{S}{C_f} \tag{23}$$

Thus, the hiding effect dimensionless parameter (i.e., D/D_g) is the only additional parameter not considered in Eq. (22).

Although selecting $\beta = 1/\sigma_t = 0.94 < 1$ accounts for the potential decrease in turbulent eddy viscosity due to high suspended tailings concentrations, which can lead to sediment stratification, it is essential to validate these β values in future experiments. These experiments could include measurements of vertical concentrations and sediment fractions throughout the water column for different u_*/v_s values.

The formulations developed herein to determine the tailings entrainment for equilibrium conditions must be carefully implemented in situations that differ from those described. One of the drawbacks to the annular flume is the relatively low shear stresses exerted on the bed material, which entrains the finer fractions into suspension. As a result, even though the tailings Samples S1 and S2 contain fractions ranging from clay to fine gravel (1.0 μm to 6.0 mm), the developed formulations should be tested against more observations with for higher bed shear stresses and a wider range of tailings grain sizes. However, due to the dimensionless nature of the formulation, and the similarity collapse of the data, one would expect that the formulation will work to estimate the resuspension of tailings with sizes and specific gravities different from those used in our experiments. Although Eqs. (20) and (21) seem to fit the measurements for sand sizes, special attention must be drawn when $R_{epi} > 30$ as Z_{ui} (and thus E_{si}) seems to increase as diameters increase.

The entrainment formulations developed for tailings beds have limitations when applied to real-world riverine systems. This is because the deposition of tailings in rivers involves a continuous mixing of the tailings with the ambient sediment material. While the density of the mixture can be measured and included in the formulations, further investigation is needed to validate their implementation for a sand-tailings mixture under riverine conditions. Because of the processes involved in mining of iron ore, the resulting tailings have sediment sizes that are oftentimes smaller than 62 micrometers, the cutoff size commonly employed to characterize the washload in sand-bed rivers. Since sand-rich rivers do not have much material finer than 62 micrometers in their bed sediment, one cannot expect that sediment entrainment functions developed for entrainment of silt and sand, will work well to estimate entrainment rates of the large fraction of fine-grained materials found in most mine tailings operations.

Likewise, we acknowledge that the experimental conditions used to develop the entrainment formulations differ from the ones that might occur in rivers. Even though flocculation and hindered settling processes were not dominant in our experiment, the properties of water in rivers (e.g., pH, water temperature) and the presence of organic matter can promote the formation of flocs in riverine systems. Additionally, the composition of tailings and the higher content of fine tailings can contribute to the formation of flocs, depending on the mineralogical content. Therefore, we emphasize that this paper is a first step in developing a general formulation for the entrainment of tailings. Further investigation is necessary to validate and adjust this equation before it can be implemented in a numerical model that aims to predict the dispersion of tailings in riverine systems. However, the proposed formulation is expected to give reasonable estimates of sediment entrainment for fine-grained tailings which behave as granular materials. This was the case for the tailings used in the experiment, which are fine-grained but consist of quartz particles (around 50%).

Conclusions

Experiments were conducted to evaluate the existing sand-based entrainment formulations derived under equilibrium conditions over two poorly sorted iron tailings samples with different GSDs and similar densities. The first set of experiments aimed to evaluate the influence of flocculation and hindered settling processes on the settling velocity for different initial and homogeneous tailings concentrations along a settling column. Based on the spatiotemporal evolution of the concentrations, we found that neither flocculation nor hindered settling processes considerably affected the settling velocities of the particles. Although hindered settling processes tend to be more dominant than flocculation (for some initial concentration conditions), we found an almost negligible influence of this process on the prediction of the near-bed tailings concentration.

The second set of experiments was conducted in an annular flume over two iron tailing samples subjected to bed shear stresses. Near-bed tailing samples were taken for each bed shear stress after reaching equilibrium conditions. Despite the high fine content in both samples, we found that the iron tailing samples behave as a noncohesive material. We also found the development of ripples and dunes during the entrainment experiments.

The results from the annular flume experiments show that the original formulations proposed by Garcia and Parker (1991), complemented by Garcia and Parker (1993), Wright and Parker (2005), and De Leeuw et al. (2020) can reasonably predict the near-bed concentrations of the iron tailings if they are treated as a well-sorted material. However, when treated as poorly sorted material (actual condition), these original sand-based entrainment formulations are not adequate for predicting the observations. To overcome this limitation, two functions (f_1 and f_2) were included in the similarity variable (Z_{ui}) proposed by Wright and Parker (2005), that depend on the dimensionless parameters R_{ep} and H/k_c.

Incorporating the first function $f_1(R_{epi})$ in the entrainment formulations is essential for particle sizes comparable to or smaller than the thickness of the viscous sublayer δ_v. This f_1 derived for poorly sorted iron tailings is similar to the one found by Garcia and Parker (1993) based on density currents over uniform-size, crushed coal bed material. This function aims to restrict the entrainment of particles within the viscous sublayer as higher turbulence is required to entrain them into the water column. However, the original function $f_1 = R_{epi}^{0.6}$ is appropriate for predicting the near-bed tailings concentrations for particles that protrude from this viscous sublayer. This transition occurs approximately when $R_{epi} = 4.5$.

The f_2 formulation is represented and included as a function of the friction coefficient C_f (i.e., $f_2(C_f)$) as this parameter depends on H/k_c. The main reason for involving f_2 in Z_{ui} is the generation of two independent clusters whose position is a function of the roughness of the tested sample. For the coarser sample, this cluster tends to be closer to the original $E_s - Z_{ui}$ curve, whereas for the fine sand- and silt-rich tailings the location of the cluster tends to overestimate the near-bed tailings concentrations.

The proposed entrainment formulation modifies the Wright and Parker (2005) equation in which f_1 and f_2 functions are included into Z_{ui}. The performance of this equation was compared with a modified formulation based on the three-parameter model formulation proposed by De Leeuw et al. (2020). Even though the latter formulation has slightly better performance, both formulations result in comparable results, and they should be limited to silt and fine sand fractions.

As long as the material behaves as granular, we expect that the proposed formulations can be implemented in a wide range of particle sizes and densities. However, we recommend performing similar analyses in flumes capable of exerting shear stresses similar to the ones typically found in riverine environments in order to generalize these formulations. It would be desirable to have suspended sediment and flow measurements from a stream with a considerable amount of tailings in its bed to validate and complement the formulations proposed in this study.

Appendix I. Bed Shear Stress Characterization

Herein we found that the ratio that minimizes the secondary currents for the walnut shells is $\Omega_L/\Omega_C = 2.2$, which differs from the ratio $\Omega_L/\Omega_C = 1.0$ found by Pedocchi (2005) for a rough lid and fixed-smooth bed conditions. The ratio $\Omega_L/\Omega_C = 2.2$ was used as a starting point to determine the Ω_L/Ω_C ratios that guarantee a relatively uniform τ_b distribution along the spanwise direction for the tailing bed conditions. Similar to the experiments conducted by Petersen and Krishnappan (1994), we identified multiple Ω_L/Ω_C ratios that meet the aforementioned condition (Fig. 14). However, we found that the relative uniform τ_b for the tailings samples was achieved when the ratio $\Omega_L/\Omega_C \sim 2.75$, which is similar to the value found by Cantero et al. (2004) based on Large Eddy Simulations (LES) conducted for a smooth ring and a fixed-smooth bottom condition. This ratio was selected to determine the rotational

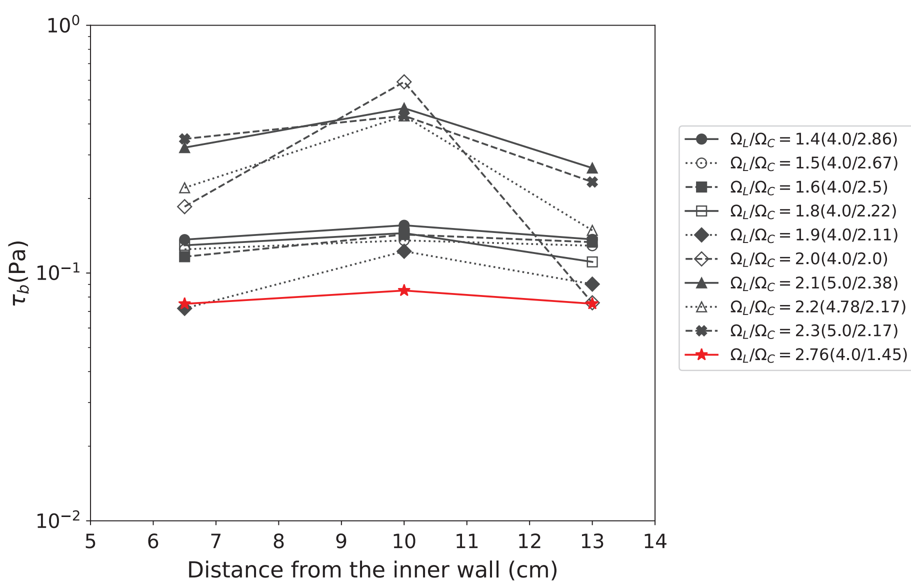

Fig. 14. (Color) Bed shear stress along the cross-section for different Ω_L/Ω_C.

J. Hydraul. Eng., 2025, 151(1): 04024065

Table 5. Friction coefficients, C_f

Parameter/sample	S1	S2	S3	Pedocchi (2005)
C_f	0.005161	0.000419	0.001588[a]	0.00014

[a]Estimated via linear interpolation based on C_f values for Samples S1 and S2.

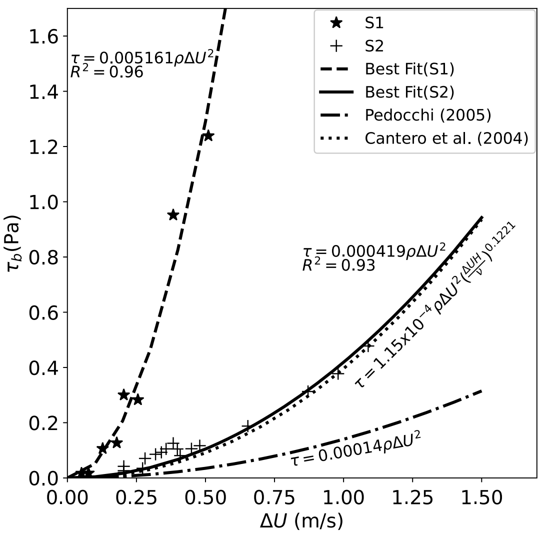

Fig. 15. Bed shear stress as a function of the tangential velocity difference between the lid and the flume for bed tailing conditions along with the equations found by Cantero et al. (2004) and Pedocchi (2005).

speeds for both the lid and the flume for the experiments in the annular flume.

For the bed tailings condition and based on the bed shear stresses τ_b estimated via TKE and the velocities of the lid and flume, we estimated the C_f for samples S1 and S2 by fitting the measurements to Eq. (10) (Table 5 and Fig. 15).

Appendix II. Settling Velocity Analysis

The settling column experiments were based on a similar settling column that Ross (1988) and Hwang and Mehta (1989) used in their experiments at the University of Florida [Eq. (24)]. In particular, we initially aimed to calibrate the parameters (a_w, a, b, d) from the equation derived by Hwang and Mehta (1989), that estimate the settling velocity of cohesive particles as a function of suspended sediment concentration

$$v_s = \begin{cases} v_{sf}, & \text{if } C < C_{fs} \\ a_w \dfrac{C^a}{(C^2+b^2)^d}, & \text{if } C_{fs} < C < C_h \\ \text{negligible}, & \text{if } C_h < C \end{cases} \tag{24}$$

where v_{sf} = free settling velocity; C = suspended sediment concentration; a_w = velocity scaling coefficient; a_s = flocculation settling exponent; b = hindered settling coefficient; d = hindered settling exponent; C_{fs} = concentration limit for free settling velocity; and C_h = concentration limit for hindered settling.

The method to calibrate the parameters from the previous equation is based on the settling column samples and a finite numerical model that solves the continuity equation for a suspension settling in quiescent water. Although we used the same procedure and a similar settling column device that Hwang and Mehta (1989) used for their experiments, we noticed that this procedure was not suitable for our experiments due to numerical instabilities. This procedure is more viable for lighter and finer samples (clay-size). Therefore, we decided to use the method proposed by McLaughlin (1958, 1959) to determine whether flocculation or hindered settling processes were important in our experiment (Vanoni 2006).

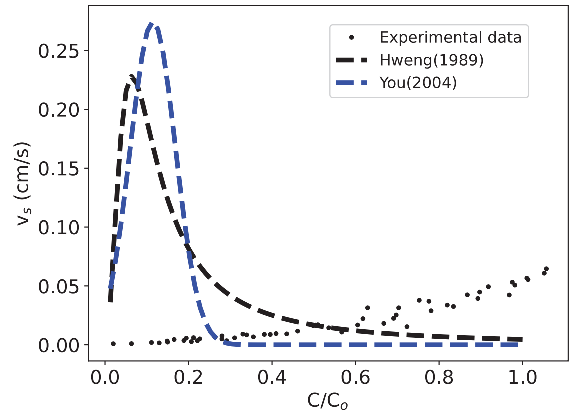

Fig. 16. (Color) Comparison of settling velocity formulas for cohesive material with observed data. The observed data was estimated based on the evolution of the D_{50} of the suspended sediment samples taken during the settling column experiments with an initial concentration of $C_0 = 16$ g/L.

In addition to the Hwang equation, we compared our experimental data with the settling velocities for cohesive materials estimated using Eq. (25) proposed by You (2004), as depicted in Fig. 16. This comparison was conducted for an initial concentration of $C_o = 16$ g/L. It is clear that the experimental data does not align with either equation, suggesting that neither flocculation nor hindered settling are significant processes in this case. Notably, the increase in settling velocity at high concentrations is attributed to the larger particle diameters settling during the initial minutes of the experiment rather than to flocculation processes. This is further demonstrated in Fig. 9(a), where the experimental data shows that the settling velocity increases with the increase in the D_{50}

$$v_s = v_{sf} e^{0.9779C - 0.1080C^2} \tag{25}$$

Data Availability Statement

All data, models, and code generated or used during the study appear in the published article.

Acknowledgments

We want to thank Associate Professor Rafael Tinoco for his valuable advice regarding the bed shear stresses characterization in the annular flume. We also want to express our gratitude to Marc Killion and Andrew Waratuke for providing technical assistance in the preparation and during the experiments. Andrés F. Rojas-Aguirre would like to thank Samuel Aguiar, Chien-Yung Tseng and Jorge San Juan for their valuable discussions, which enhanced the quality of this research. Finally, we thank Leila Hernández, Pallav Ranjan, Vindhyawasini Prasad, Juan Andrade, Kevin Wallington, and Manuel Reyna for their help in taking samples during the settling column experiments. The financial support and resources provided by the M.T. Geoffrey Yeh Chair in Civil Engineering are gratefully acknowledged.

Notation

The following symbols are used in this paper:

A_d = mean absolute deviation of the discrepancy ratio;
a = reference height;
a_s = flocculation settling exponent;
a_w = velocity scaling coefficient;
b = hindered settling coefficient;
C = total and local particle concentration;
C_a = total near-bed concentration at reference height a;
C_{ai} = near-bed concentration of grain size i at reference height a;
C_D = drag coefficient;
C_f = dimensionless bed friction coefficient;
C_{fs} = concentration limit for free settling velocity;
C_h = concentration limit for hindered settling;
C_o = initial concentration for the settling column experiments;
C_{zi} = volumetric sediment concentration at z;
C_1, C_2 = constants for Eq. (8);
C_3 = constant ranges between 0.18 to 0.20;
D_g = geometric mean size;
D_i = diameter of grain size i;
D_r = settling flux;
D_{50} = grain size for which 50% of the material is finer;
D^* = dimensionless particle diameter;
E = erosion rate;
E_r = erosion flux;
E_{si} = entrainment of grain size i;
F = upward volume flux of suspended sediment;
F_i = volume fraction of grain size i in bed material;
Fr = Froude number;
f_{ai} = volume fraction of grain size i in the suspended material at reference height a;
g = acceleration of gravity;
H = water depth;
H_d = hydraulic depth;
k_s = grain roughness;
M_e = mean of the discrepancy ratio;
RSS = residual sum of squares;
R_{epi} = particle Reynolds number of grain size i;
R_h = hydraulic radius;
R_i = submerged specific gravity of grain size i;
S = longitudinal slope;
TKE = turbulent kinetic energy;
t = time;
U = mean velocity;
U_{FL} = velocity difference between lid and flume;
U_r = mean velocity without bedforms within $z = [k_s, \Delta_l]$;
u' = velocity fluctuation in the tangential direction;
u_* = shear velocity;
u_s^* = skin friction component of the shear velocity;
x = tangential coordinate;
y = radial coordinate;
Z_i = rouse number of grain size i;
Z_{ui} = similarity variable of grain size i;
z = vertical coordinate;
z' = velocity fluctuation in the vertical direction;
α = coefficient determined by erosion experiments;
β = dimensionless parameter that relates the coefficient for momentum exchange with the diffusion coefficient;
Δ_{FL} = velocity difference between the lid and the flume;
Δ_l = dune amplitude;
δ_v = thickness of the viscous sublayer;
ϵ_m = turbulent diffusivity of the sediment;
η = channel bed elevation;
θ = coefficient determined by erosion experiments;
κ = von Karman's constant;
λ = parameter that characterizes mixture suppression of entrainment;
λ_l = dune wavelength;
ρ = water density;
σ_t = Schmidt number;
σ_Φ = geometric standard deviation of bed material;
τ_b = total bed shear stress;
τ_{bf} = form drag component of the total bed shear stress;
τ_{bs} = skin component of the total bed shear stress;
τ_{bi}^* = dimensionless bed shear stress of grain size i;
τ_{cr}^* = critical shear stress;
ν = kinematic viscosity;
v_{sf} = free settling velocity of grain size i;
v_{si} = settling velocity of grain size i;
ν_t = turbulent eddy viscosity;
v' = velocity fluctuation in the radial direction;
ϕ_{fines} = content of fines;
Ω_C = angular velocity of the flume; and
Ω_L = angular velocity of the lid.

Supplemental Materials

There are Supplemental Materials associated with this paper online in the ASCE Library (www.ascelibrary.org).

References

Adu-Wusu, C., E. K. Yanful, and M. H. Mian. 2001. "Field evidence of resuspension in a mine tailings pond." *Can. Geotech. J.* 38 (4): 796–808. https://doi.org/10.1139/t01-005.

Akiyama, J., and Y. Fukushima. 1986. "Entrainment of noncohesive bed sediment into suspension." In Vol. 3 of *Proc., 3rd Int. Symp. on River Sedimentation, Central Theme, Estuarine and Coastal Sedimentation*, edited by S. Y. Wang, H. W. Shen, and L. Z. Ding, 804–813. University, MS: Mississippi Univ.

Ariathurai, R., and R. B. Krone. 1976. "Finite element model for cohesive sediment transport." *J. Hydraul. Div.* 102 (3): 323–338. https://doi.org/10.1061/JYCEAJ.0004489.

Armstrong, M., R. Petter, and C. Petter. 2019. "Why have so many tailings dams failed in recent years?" *Resour. Policy* 63 (Oct): 101412. https://doi.org/10.1016/j.resourpol.2019.101412.

ASTM. 2014. *Standard test methods for specific gravity of soil solids by water pycnometer*. ASTM D854-14. West Conshohocken, PA: ASTM.

ASTM. 2017a. *Standard test method for particle-size distribution (gradation) of fine-grained soils using the sedimentation (hydrometer) analysis*. ASTM D7928-17. West Conshohocken, PA: ASTM.

ASTM. 2017b. *Standard test methods for particle-size distribution (gradation) of soils using sieve analysis*. ASTM D6913/D6913M-17. West Conshohocken, PA: ASTM.

ASTM. 2019. *Standard test methods for determining sediment concentration in water samples*. ASTM D3977-97(2019). West Conshohocken, PA: ASTM.

Azam, S., and Q. Li. 2010. "Tailings dam failures: A review of the last one hundred years." *Geotech. News* 28 (4): 50–53.

Booij, R. 1994. *Measurement of the flow field in a rotating annular flume*. Rep. No. 94-2. Delft, Netherlands: Faculty of Civil Engineering, Delft Univ. of Technology.

Cantero, M., S. Mangini, F. Pedocchi, Y. Niño, and M. H. Garcia. 2004. "Analysis of flow characteristics in an annular flume: Implications for erosion and deposition of cohesive sediments." In *Proc., World Water and Environmental Resources Congress 2004*, 1–10. Reston, VA: ASCE. https://doi.org/10.1061/40737(2004)314.

Cao, Z., and G. Pender. 2004. "Numerical modelling of alluvial rivers subject to interactive sediment mining and feeding." *Adv. Water Resour.* 27 (5): 533–546. https://doi.org/10.1016/j.advwatres.2004.02.017.

De Leeuw, J., M. P. Lamb, G. Parker, A. J. Moodie, D. Haught, J. G. Venditti, and J. A. Nittrouer. 2020. "Entrainment and suspension of sand and gravel." *Earth Surf. Dyn.* 8 (2): 485–504. https://doi.org/10.5194/esurf-8-485-2020.

do Carmo, F. F., et al. 2017. "Fundão tailings dam failures: The environment tragedy of the largest technological disaster of Brazilian mining in global context." *Perspect. Ecol. Conserv.* 15 (3): 145–151. https://doi.org/10.1016/j.pecon.2017.06.002.

Ferguson, R. I., and M. Church. 2004. "A simple universal equation for grain settling velocity." *J. Sediment. Res.* 74 (6): 933–937. https://doi.org/10.1306/051204740933.

Fernández, R., M. H. García, and G. Parker. 2018. "Upper Mississippi River flow and sediment characteristics and their effect on a harbor siltation case." *J. Hydraul. Eng.* 144 (10): 04018066. https://doi.org/10.1061/(ASCE)HY.1943-7900.0001507.

Fredsøe, J., and R. Deigaard. 1992. *Mechanics of coastal sediment transport*. Singapore: World Scientific.

Garcia, M., and G. Parker. 1991. "Entrainment of bed sediment into suspension." *J. Hydraul. Eng.* 117 (4): 414–435. https://doi.org/10.1061/(ASCE)0733-9429(1991)117:4(414).

Garcia, M. H. 2008. "Sediment transport and morphodynamics." Chap. 2 in *Sedimentation engineering: Processes, measurements, modeling, and practice*, edited by M. H. Garcia, 21–163. Reston, VA: ASCE.

Garcia, M. H., and G. Parker. 1993. "Experiments on the entrainment of sediment into suspension by a dense bottom current." *J. Geophys. Res.: Oceans* 98 (C3): 4793–4807. https://doi.org/10.1029/92JC02404.

Geremew, A. M. 2017. "Erosion characteristics and stochastic nature of bed shear stress in underwater mine tailings." *Can. J. Civ. Eng.* 44 (6): 426–440. https://doi.org/10.1139/cjce-2016-0319.

Geremew, A. M., and E. K. Yanful. 2011. "Role of fines on cohesive behavior of mine tailings inferred from critical shear stress." *Can. Geotech. J.* 48 (4): 568–582. https://doi.org/10.1139/t10-089.

Ghahramani, N., H. J. Chen, D. Clohan, S. Liu, M. Llano-Serna, N. M. Rana, S. McDougall, S. G. Evans, and W. A. Take. 2022. "A benchmarking study of four numerical runout models for the simulation of tailings flows." *Sci. Total Environ.* 827 (Jun): 154245. https://doi.org/10.1016/j.scitotenv.2022.154245.

Graf, W. H., and M. Cellino. 2010. "Suspension flows in open channels; experimental study." *J. Hydraul. Res.* 40 (4): 435–447. https://doi.org/10.1080/00221680209499886.

Haneef-Mian, M., E. K. Yanful, and R. Martinuzzi. 2007. "Measuring the onset of mine tailings erosion." *Can. Geotech. J.* 44 (4): 473–489. https://doi.org/10.1139/t06-116.

Hayter, E. J., and A. J. Mehta. 1986. "Modelling cohesive sediment transport in estuarial waters." *Appl. Math. Modell.* 10 (4): 294–303. https://doi.org/10.1016/0307-904X(86)90061-2.

Hudson-Edwards, K. A., M. G. Macklin, H. E. Jamieson, P. A. Brewer, T. J. Coulthard, A. J. Howard, and J. N. Turner. 2003. "The impact of tailings dam spills and clean-up operations on sediment and water quality in river systems: The Ríos Agrio-Guadiamar, Aznalcóllar, Spain." *Appl. Geochem.* 18 (2): 221–239. https://doi.org/10.1016/S0883-2927(02)00122-1.

Hwang, K.-N., and A. J. Mehta. 1989. *Fine sediment erodibility in Lake Okeechobee, Florida*. Rep. No. UFL/COEL-89/019. Gainesville, FL: South Florida Water Management District, Univ. of Florida.

ICOLD (International Committee of Large Dams). 2001. "Tailings dams–risk of dangerous occurrences. Lessons learnt from practical experiences (bulletin 121)." Accessed January 16, 2024. http://www.icold-cigb.org.

Lumbroso, D., M. Davison, R. Body, and G. Petkovšek. 2021. "Modelling the Brumadinho tailings dam failure, the subsequent loss of life and how it could have been reduced." *Nat. Hazards Earth Syst. Sci.* 21 (1): 21–37. https://doi.org/10.5194/nhess-21-21-2021.

Lyn, D. 2008. "Turbulence models for sediment transport engineering." Chap. 16 in *Sedimentation engineering: Processes, measurements, modeling, and practice*, 761–824. Reston, VA: ASCE.

Macklin, M. G., P. A. Brewer, D. Balteanu, T. J. Coulthard, B. Driga, A. J. Howard, and S. Zaharia. 2003. "The long term fate and environmental significance of contaminant metals released by the January and March 2000 mining tailings dam failures in Maramures County, upper Tisa Basin, Romania." *Appl. Geochem.* 18 (2): 241–257. https://doi.org/10.1016/S0883-2927(02)00123-3.

Martínez-Aranda, S., R. García, and P. García-Navarro. 2022. "GPU-accelerated developments for the realistic simulation of large-scale mud/debris flows." Accessed June 13, 2024. https://www.iahr.org/library/infor?pid=21249.

McLaughlin, R. T. 1958. "On the mechanics of sedimentation in artificial basins." Ph.D. thesis, Dept. of Engineering and Applied Science, California Institute of Technology.

McLaughlin, R. T. 1959. "The settling properties of suspensions." *J. Hydraul. Div.* 85 (12): 9–41. https://doi.org/10.1061/JYCEAJ.0000382.

McLean, S. R. 1991. "Depth-integrated suspended-load calculations." *J. Hydraul. Eng.* 117 (11): 1440–1458. https://doi.org/10.1061/(ASCE)0733-9429(1991)117:11(1440).

Mehta, A. J. 1973. "Depositional behavior of cohesive sediments." Ph.D. thesis, Dept. of Civil and Coastal Engineering, Univ. of Florida.

Mehta, A. J., and W. H. McAnally. 2008. "Fine grained sediment transport." Chap. 4 in *Sedimentation engineering: Processes, measurements, modeling, and practice*, 253–306. Reston, VA: ASCE.

Mian, M. H., and E. K. Yanful. 2004. "Analysis of wind-driven resuspension of metal mine sludge in a tailings pond." *J. Environ. Eng. Sci.* 3 (2): 119–135. https://doi.org/10.1139/s03-076.

Nelson, J. M., and J. D. Smith. 1989. "Flow in meandering channels with natural topography." In Vol. 12 of *River meandering*, 69–102. Washington, DC: American Geophysical Union.

Nino, Y., F. Lopez, and M. Garcia. 2003. "Threshold for particle entrainment into suspension." *Sedimentology* 50 (2): 247–263. https://doi.org/10.1046/j.1365-3091.2003.00551.x.

Parker, G., and A. G. Anderson. 1977. "Basic principles of river hydraulics." *J. Hydraul. Div.* 103 (9): 1077–1087. https://doi.org/10.1061/JYCEAJ.0004827.

Partheniades, E., J. F. Kennedy, R. J. Etter, and R. P. Hoyer. 1966. *Investigation of the depositional behavior of fine cohesive sediments in an annular rotating channel*. Rep. No. 96. Cambridge, MA: Massachusetts Institute of Technology.

Pedocchi, F. 2005. "Evaluation of laser diffraction instrument and an annular flume for cohesive sediment studies." Master's thesis, Dept. of Civil and Environmental Engineering, Univ. of Illinois at Urbana-Champaign.

Petersen, O., and B. G. Krishnappan. 1994. "Measurement and analysis of flow characteristics in a rotating circular flume: Mésure et analyse de l'ecoulement dan un canal circulaire rotatif." *J. Hydraul. Res.* 32 (4): 483–494. https://doi.org/10.1080/00221686.1994.9728351.

Piciullo, L., E. B. Storrøsten, Z. Liu, F. Nadim, and S. Lacasse. 2022. "A new look at the statistics of tailings dam failures." *Eng. Geol.* 303 (Jun): 106657. https://doi.org/10.1016/j.enggeo.2022.106657.

Pickup, G., and Y. Cui. 2008. "Chapter 7 modeling the impact of tailings and waste rock disposal on the fly river system." *Dev. Earth Environ. Sci.* 9 (Jan): 257–289. https://doi.org/10.1016/S1571-9197(08)00407-2.

Pope, N. D. Ã., J. Widdows, and M. D. Brinsley. 2006. "Estimation of bed shear stress using the turbulent kinetic energy approach—A comparison of annular flume and field data." *Cont. Shelf Res.* 26 (8): 959–970. https://doi.org/10.1016/j.csr.2006.02.010.

Ross, A. M. 1988. "Vertical structure of estuarine fine sediment suspensions." Ph.D. thesis, Coastal and Oceanographic Engineering Dept., Univ. of Florida.

San Juan, J. E. 2016. "Radial and tangential velocity profiles in an annular flume." M.S. thesis, Dept. of Civil and Environmental Engineering, Univ. of Illinois at Urbana-Champaign.

Simeoni, L., G. Tosatti, G. Lucchi, and M. Longo. 2017. "The Stava catastrophic failure of July 19, 1985 (Italy): Technical-scientific data and socioeconomic aspects." *CSE J. City Saf. Energy* 1985 (1): 17–30.

Smith, J. D., and S. R. McLean. 1977. "Spatially averaged flow over a wavy surface." *J. Geophys. Res.* 82 (12): 1735–1746. https://doi.org/10.1029/JC082i012p01735.

Soulsby, R. L. 1983. "Chapter 5 the bottom boundary layer of shelf seas." *Elsevier Oceanogr. Ser.* 35: 189–266. https://doi.org/10.1016/S0422-9894(08)70503-8.

Thompson, C. E., C. L. Amos, T. E. Jones, and J. Chaplin. 2003. "The manifestation of fluid-transmitted bed shear stress in a smooth annular flume—A comparison of methods." *J. Coastal Res.* 19 (4): 1094–1103.

Thompson, F., et al. 2020. "Severe impacts of the Brumadinho dam failure (Minas Gerais, Brazil) on the water quality of the Paraopeba River." *Sci. Total Environ.* 705 (Feb): 135914. https://doi.org/10.1016/j.scitotenv.2019.135914.

UIUC and MWRDGC (University of Illinois at Urbana Champaign and Metropolitan Water Reclamation District of Greater Chicago). 2003. *Sedimentation management in combined sewer overflow storage reservoirs using water jets*. Rep. No. HES 76. Chicago: UIUC and MWRDGC.

UIUC (University of Illinois at Urbana-Champaign). 2005. *Erosional properties of mine tailing lake Wabush, Labrador, Canada*. Rep. No. 1969. Champaign, IL: UIUC.

UNEP (United Nations Environment Programme). 1996. *Environmental and safety incidents concerning tailings dams at mines. results of a survey for the years 1980–1996*. Nairobi, Kenya: UNEP.

Vanoni, V. A. 2006. *Sedimentation engineering*. Classic ed. Reston, VA: ASCE.

van Rijn, L. C. 1984. "Sediment transport, Part II: Suspended load transport." *J. Hydraul. Eng.* 110 (11): 1613–1641. https://doi.org/10.1061/(ASCE)0733-9429(1984)110:11(1613).

Wei, H., Y. K. Liu, H. L. Wu, and Y. Y. Wan. 2017. "The incipient motion features of sediment from Yangtze estuary: Annular flume experiments." *Sci. Rep.* 7 (1): 13285. https://doi.org/10.1038/s41598-017-13651-2.

WISE (World Information Service on Energy). 2022. "Chronology of tailings dam failures." *WISE Uranium Project*. Accessed January 30, 2024. https://www.wise-uranium.org/mdaf.html.

Wright, S., and G. Parker. 2003. "Grain-size specific suspended sediment transport and flow resistance in large sand-bed rivers." In *Proc., Sedimentation and Sediment Transport: Proc. of the Symp. Held in Monte Verità, Switzerland*, 221–227. Dordrecht, Netherlands: Springer.

Wright, S., and G. Parker. 2005. "Flow resistance and suspended load in sand-bed rivers: Simplified stratification model." *J. Hydraul. Eng.* 130 (8): 796–805. https://doi.org/10.1061/(ASCE)0733-9429(2004)130:8(796).

Yanful, E. K., and L. J. J. Catalan. 2002. "Predicted and field-measured resuspension of flooded mine tailings." *J. Environ. Eng.* 128 (4): 341–351. https://doi.org/10.1061/(ASCE)0733-9372(2002)128:4(341).

Yang, Z., A. Baptista, and J. Darland. 2000. "Numerical modeling of flow characteristics in a rotating annular flume." *Dyn. Atmos. Oceans* 31 (1–4): 271–294. https://doi.org/10.1016/S0377-0265(99)00037-8.

You, Z. J. 2004. "The effect of suspended sediment concentration on the settling velocity of cohesive sediment in quiescent water." *Ocean Eng.* 31 (16): 1955–1965. https://doi.org/10.1016/j.oceaneng.2004.05.005.

Zyserman, J. A., and J. Fredsøe. 1994. "Data analysis of bed concentration of suspended sediment." *J. Hydraul. Eng.* 120 (9): 1021–1042. https://doi.org/10.1061/(ASCE)0733-9429(1994)120:9(1021).

J. Hydraul. Eng., 2025, 151(1): 04024065